Septin ring size scaling and dynamics require the coiled-coil region of Shs1p

Rebecca A. Meseroll[a], Louisa Howard[b], and Amy S. Gladfelter[a]
[a]Department of Biological Sciences and [b]EM Facility, Dartmouth College, Hanover, NH 03755

ABSTRACT **Septins are conserved GTP-binding proteins that assemble into heteromeric complexes that form filaments and higher-order structures in cells. What directs filament assembly, determines the size of higher-order septin structures, and governs septin dynamics is still not well understood. We previously identified two kinases essential for septin ring assembly in the filamentous fungus *Ashbya gossypii* and demonstrate here that the septin Shs1p is multiphosphorylated at the C-terminus of the protein near the predicted coiled-coil domain. Expression of the nonphosphorylatable allele *shs1*-9A does not mimic the loss of the kinase nor does complete truncation of the Shs1p C-terminus. Surprisingly, however, loss of the C-terminus or the predicted coiled-coil domain of Shs1p generates expanded zones of septin assemblies and ectopic septin fibers, as well as aberrant cell morphology. The expanded structures form coincident with ring assembly and are heteromeric. Interestingly, while septin recruitment to convex membranes is increased, septin localization is diminished at concave membranes in these mutants. Additionally, the loss of the coiled-coil leads to increased mobility of Shs1p. These data indicate the coiled-coil of Shs1p is an important negative regulator of septin ring size and mobility, and its absence may make septin assembly sensitive to local membrane curvature.**

Monitoring Editor
Gero Steinberg
University of Exeter

Received: Mar 13, 2012
Revised: Jun 15, 2012
Accepted: Jun 27, 2012

INTRODUCTION

The septins are a class of conserved eukaryotic cytoskeletal proteins that assemble into heteromeric filaments and higher-order structures in vivo (Beise and Trimble, 2011; Oh and Bi, 2011; Mostowy and Cossart, 2012). They were first discovered in budding yeast to be required for cytokinesis (Hartwell, 1971) and have since been shown to participate in many cellular functions, including exocytosis, apoptosis, and membrane compartmentalization (Barral *et al.*, 2000; Takizawa *et al.*, 2000; Luedeke *et al.*, 2005; Amin *et al.*, 2008; McMurray *et al.*, 2011b). Septins can also act as scaffolds whose purpose is to recruit signaling molecules to a specific place at a specific time (Gladfelter *et al.*, 2001; Hagiwara *et al.*, 2011). Misexpressed or dysfunctional septins in humans are associated with several neurological disorders, including Alzheimer's and Parkinson's diseases (Kinoshita *et al.*, 1998; Ihara *et al.*, 2007), and with many different types of cancer (Peterson and Petty, 2010).

The formation of septins into heteromeric complexes and higher-order structures is tightly linked to septin function (McMurray *et al.*, 2011a). Recombinant or purified septins can self-assemble in vitro into nonpolar heteromeric complexes that spontaneously polymerize into long, frequently paired, filaments under low-salt conditions (Field *et al.*, 1996; Frazier *et al.*, 1998). Under high-salt conditions that inhibit the polymerization of recombinant septin complexes into filaments in solution, the presence of phosphatidylinositol-4,5-bisphosphate (PIP_2) membranes promotes polymerization and assembly of crossed networks of filaments (Bertin *et al.*, 2010), indicating a role for membranes in septin filament formation. In vivo, septins organize into various higher-order structures, such as rings, bars, and gauzes (Kinoshita *et al.*, 2002; Rodal *et al.*, 2005; DeMay *et al.*, 2011). These higher-order structures are often associated with the cell cortex, and their formation at the correct time and place is

This article was published online ahead of print in MBoC in Press (http://www.molbiolcell.org/cgi/doi/10.1091/mbc.E12-03-0207) on July 5, 2012.

Address correspondence to: Amy S. Gladfelter (amy.gladfelter@dartmouth.edu).

Abbreviations used: *Ag* Shs1ΔC-GFP, *Ashbya gossypii* Shs1ΔC-GFP; CCD, charge-coupled device; EGTA, ethylene glycol tetraacetic acid; FCF, forchlorfenuron; FRAP, fluorescence recovery after photobleaching; IgG, immunoglobulin G; IR, interregion; NA, numerical aperture; ORF, open reading frame; PIP_2, phosphatidylinositol-4,5-bisphosphate; PVDF, polyvinylidene fluoride; *Sc SHS1*, *S. cerevisiae SHS1*; Shs1-GFP, Shs1–green fluorescent protein.

required for normal septin function. Many aspects of septin assembly in the cell remain mysterious: How do septin filaments assemble into higher-order structures? What directs the size and shape of the structures? How does the local geometry of the cell cortex influence the formation and persistence of septin assemblies?

It has been shown that the septins interact with one another and membranes via a series of conserved domains. In general, the septins are made up of a variable N-terminal region with a polybasic domain, which may contribute to septin–membrane interactions; a central GTP-binding domain; and a variable C-terminal extension that sometimes includes a predicted coiled-coil domain (Casamayor and Snyder, 2003; Beise and Trimble, 2011). The crystal structure of the mammalian Sept2, 6, 7 complex revealed that the septins interact with one another via an interface encompassing the G domain and an interface comprising the N- and C-termini (Sirajuddin *et al.*, 2007). GTP binding contributes to septin–septin interactions and complex formation (Nagaraj *et al.*, 2008; Bertin *et al.*, 2010). The order of septin subunits in complexes and filaments is determined by which interface a given septin subunit associates with another septin subunit. The ability to oligomerize and form filaments via these interfaces is necessary to form higher-order septin structures and has been shown to be essential for function in budding yeast (McMurray *et al.*, 2011a).

Based on electron microscopy data showing paired septin filaments with a periodic electron density between the pairs, akin to railroad tracks, it has been suggested that coiled-coil domains of the septins may be playing a role in linking filaments (Bertin *et al.*, 2008). However, recombinantly expressed yeast septin complexes lacking their coiled-coil domains were shown to be capable of paired filament formation in vitro on PIP_2-containing membranes but unable to form extended lateral or crossing associations to make septin meshes (Bertin *et al.*, 2010). Because different septin subunits neighbor one another in the yeast septin complex, heteromeric coiled-coil interactions could help stabilize formation of septin protofilaments in the absence of membranes (Bertin *et al.*, 2008, 2010; de Almeida Marques *et al.*, 2012). It is still unknown where the coiled-coils are oriented relative to septin filaments or with respect to membrane surfaces. Thus, the precise role of coiled-coil domains in septin organization and the mechanisms by which the oligomers and filaments assemble into higher-order structures in cells remain unclear.

In this study, we are using *Ashbya gossypii* as a model for studying septin higher-order structure formation (Dietrich *et al.*, 2004). *Ashbya* has three distinct septin structures: a diffuse cloud at the tips of growing hyphae, cortically associated rings at the interregion (IR) of the cell, and rings around the cortex of branch sites (DeMay *et al.*, 2009). Unlike septin rings that form at the mother-bud neck of yeast, the septin rings that form at the *Ashbya* IR and branches are composed of discrete bars of septin filaments, persist over many hours, and are not influenced by the cell cycle (DeMay *et al.*, 2009). Like yeast, *Ashbya* expresses five septins during vegetative growth, Cdc3p, Cdc10p, Cdc11p, Cdc12p, and Shs1p (Sep7p), and all are essential for ring formation (DeMay *et al.*, 2009). In yeast, however, Shs1p is dispensable for septin ring assembly, whereas the other septins are essential for ring formation, dependent somewhat on strain background (Iwase *et al.*, 2007; Garcia *et al.*, 2011; McMurray *et al.*, 2011a).

Several studies have shown that posttranslational modifications to the septins, including phosphorylation, sumoylation, and acetylation, play a role in normal septin organization (Johnson and Blobel, 1999; Mortensen *et al.*, 2002; Tang and Reed, 2002; Sinha *et al.*, 2007; Egelhofer *et al.*, 2008; Mitchell *et al.*, 2011). We previously identified a pair of kinases, Elm1p and Gin4p, that are required for assembly of septin rings in the filamentous fungus *A. gossypii* (DeMay *et al.*, 2009). In the absence of either of these kinases, septins localizing as a diffuse cloud to the tips of growing hyphae cannot assemble into cortically attached rings. We show that the septin subunit Shs1p has multiple phosphorylation sites in its C-terminus in proximity to the predicted coiled-coil domain. This makes the Shs1p C-terminus an appealing potential regulatory region for septin filament and higher-order structure formation. Data presented in this study demonstrate that the C-terminal coiled-coil domain of Shs1p, but surprisingly not phosphorylation, is required to limit septin ring size and mobility within higher-order assemblies.

RESULTS

The C-terminus of Shs1p is a candidate regulatory region

We hypothesized that phosphorylation of septins may regulate septin assembly because *Ashbya* cells lacking the Elm1p or Gin4p kinases have defects building higher-order rings (DeMay *et al.*, 2009). Immunoprecipitation of the septin Shs1p indicated this septin migrates at a higher than predicted molecular weight (~75–85 kDa, as opposed to the 65 kDa predicted by primary sequence) as monitored by SDS–PAGE (Figure 1A). This mobility shift is eliminated when immunoprecipitated Shs1p is treated with phosphatase (Figure 1A). The high-molecular-weight Shs1–green fluorescent protein (Shs1-GFP; migrating at 100–110 kDa) associates with the other four septins, Cdc3p, Cdc11p, Cdc12p, and Cdc10p (Figure 1B), indicating *Ashbya* septins form heteromeric complexes composed of five different septin subunits. In vitro, these purified complexes form protofilaments that are on average 32.8 ± 4.3 nm (n = 529), suggesting *Ashbya* septin protofilaments, like those purified from yeast (Frazier *et al.*, 1998), are generally octameric, given an individual subunit length of approximately 4 nm (Figure 1, C, left, and D). Interestingly, yeast protofilament lengths were measured for complexes composed of only four of the septin subunits (Frazier *et al.*, 1998), yet the purified *Ashbya* complex represents all five septin subunits. On incubation in a low-salt solution, the septin complexes were able to polymerize into paired filaments (Figure 1C, right).

For determination of which sites are modified on Shs1p, both bands corresponding to the size of Shs1-GFP were cut out and submitted for mass spectrometry analysis. We found that Shs1-GFP is phosphorylated at nine sites (Ser-359, Ser-362, Ser-380, Thr-394, Ser-396, Ser-408, Ser-431, Thr-555, Ser-558) in the C-terminus of the protein, but is neither acetylated nor sumoylated. These phosphorylation sites lie in proximity to, but not within, the predicted coiled-coil domain (Figure 1E). Thus, the C-terminus, encompassing the phosphorylation sites and the coiled-coil domain, is an attractive candidate region for examining the regulation of Shs1p and septin ring assembly.

Loss of the Shs1p C-terminus leads to aberrant, temperature-sensitive septin assemblies

For evaluation of the role of the C-terminus of Shs1p in higher-order septin structure and function, *SHS1* was truncated at the first phosphorylation site (Ser-359, as indicated in the Shs1ΔC schematic, Figure 1E), tagged with GFP, and expressed as the only copy of the allele at the endogenous locus of *SHS1*. Surprisingly, loss of the Shs1p C-terminus (residues 359–580), encompassing all of the phosphorylation sites as well as the coiled-coil domain, did not lead to a loss of septin rings. Septin rings are still able to form at branch sites and throughout the IR of the cell (Figure 2, A and B). However, branch rings with Shs1ΔC-GFP are larger and are made of whisker-like, elongated fibers that follow the convex cell cortex. These cortical

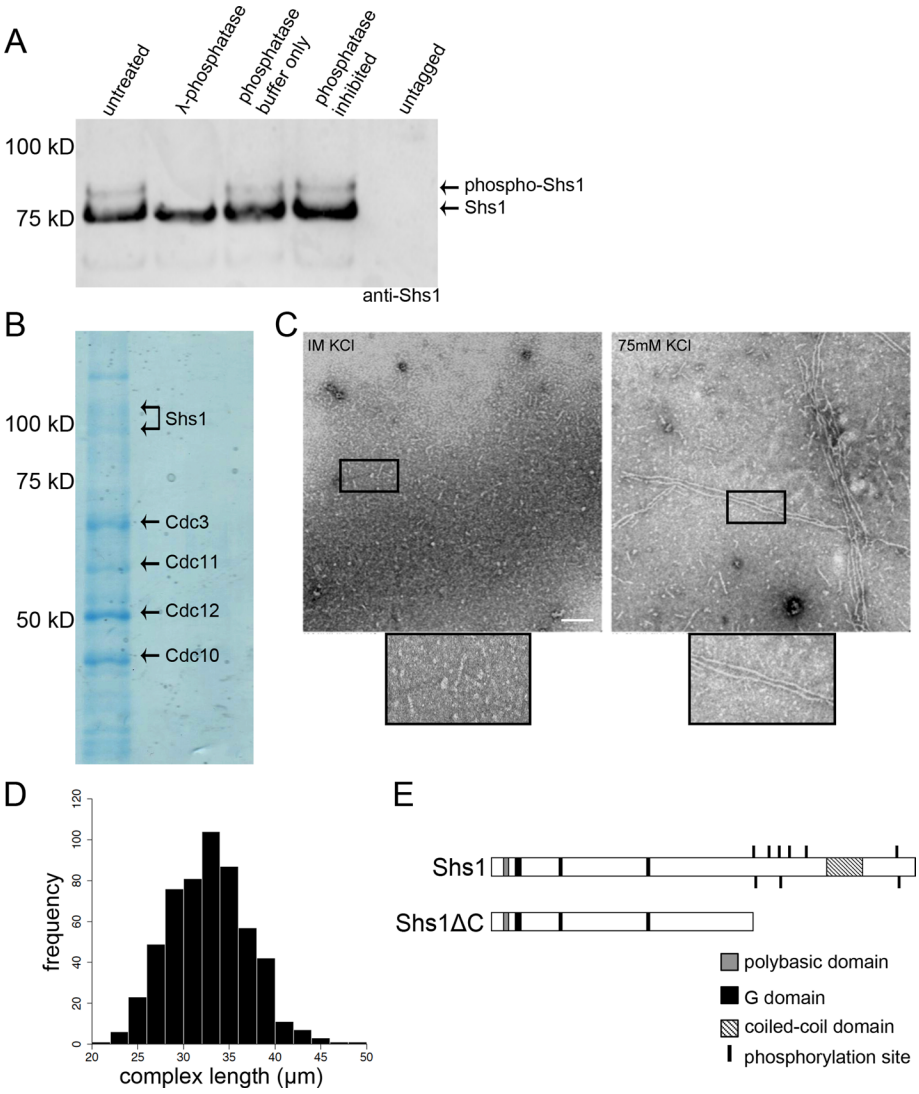

FIGURE 1: The Shs1p C-terminus is a candidate regulatory region. (A) Shs1p is phosphorylated. Cdc11-TAP was immunoprecipitated from *Ashbya* lysates (AG495.1) to pull down the entire septin complex. The immunoprecipitate was treated with λ-phosphatase, phosphatase buffer only, or phosphatase buffer with phosphatase inhibitors. Proteins were separated on SDS–PAGE, transferred to PVDF membrane, and probed with anti-Shs1 antibody. (B) Purification of the septin complex. Shs1-GFP was immunoprecipitated from *Ashbya* lysates (AG124) using the GFP-Trap-M system. Proteins were separated on SDS–PAGE and stained with colloidal-blue stain. (C) *Ashbya* septins form filaments in vitro. Cdc11-TAP was immunoprecipitated from *Ashbya* (AG495.1) to precipitate the entire complex. The complex was separated from protein A–Sepharose beads using TEV protease. Protein complexes were transferred to carbon grids and negatively stained with uranyl acetate. Boxes have been enlarged to show individual complexes in 1M KCl and filaments in 75 mM KCl solutions. Scale bar: 100 nm. (D) Distribution of septin complex lengths in 1 M KCl solutions. Mean complex length is 32.8 ± 4.3 nm, consistent with octameric complexes. $n = 529$ complexes. (E) Schematics for full-length Shs1p and the C-terminal truncation mutant, Shs1ΔC.

structures can be seen in cross-section as individual, expanded bars encircling the bases of branches and continuing along the main hypha (Figure 2B, bottom panels). This mutant thus extends the size of septin structures specifically associated with the curved membrane of lateral branches. Ectopic fibers of Shs1ΔC-GFP are also found at the cortex throughout the IR (Figure 2, A and B). Shs1ΔC-GFP is expressed at levels comparable with those of Shs1-GFP, indicating that enhanced levels of Shs1ΔC-GFP are not leading to the increased zones of assembly and additional septin fibers we see in the mutant strain (Figure 2C). Interestingly, these fibers do not form if Shs1ΔC-GFP is expressed in a strain with a wild-type Shs1p, indicating this allele is recessive (Supplemental Figure S1).

We tested the stability of expanded branch rings and ectopic filaments in the Shs1ΔC mutant by growing cells at 37°C overnight. At this temperature, septin rings are normally able to form and persist. However, as shown in Figure 2D, for cells expressing the Shs1p C-terminal truncation, there is a decrease in the frequency of enlarged branch rings (64% at 30°C compared with 42% at 37°C, $n > 20$ rings each). This indicates that the expanded structures are defective in assembly or are relatively unstable compared with the normal rings at high temperature, although overall expression levels are unchanged for Shs1ΔC-GFP compared with Shs1-GFP (Figure 2E). This is especially interesting, because even though Shs1ΔC-GFP is incorporating into the branch and IR rings in the mutant strains, these "normal"-sized rings do not appear to be affected by the increase in temperature; only the expansion zones and elongated fibers appear to be affected. It is possible that the increased temperature alters membrane composition such that the zone of septin recruitment to the cortex is more limited at high temperature.

Loss of the Shs1p C-terminus impacts cell morphology

To determine whether there were functional consequences of the expanded septin structures, we assessed cell morphology in *shs1ΔC* mutants. Introduction of Shs1ΔC-GFP led to a slight, but statistically significant, defect in colony growth (Figure 3A; $p < 0.05$), but did not affect ascospore production, a process that requires septins. Looking at individual cells, it was apparent that the loss of the Shs1p C-terminus had an effect on overall cell morphology (Figure 3B). The hyphae of this mutant appear swollen, possessing average hyphal widths 0.5-μm wider than those seen in wild-type cells (Figure 3C, left; $n \geq 196$ hyphae each; $p < 0.0001$). Additionally, Shs1ΔC cells form branches more frequently, with an average interbranch distance of 11.0 ± 7.2 μm, compared with 15.5 ± 10.9 μm average distance between branches for the wild-type (Figure 3C, right; $n > 300$ distances each strain; $p < 0.0001$).

These cell morphological defects are not a result of an alteration in the actin cytoskeleton. Actin patches are heavily concentrated at the same percentage of hyphal tips (86% for both strains) with a comparable relative mean fluorescence intensity for a given volume for both the wild-type (57.8 ± 18.0 a.u., $n = 99$) and the mutant (56.1 ± 17 a.u., $n = 76$, Figure 3D). This suggests that while there is an increase in branch frequency, there is no deficiency in actin

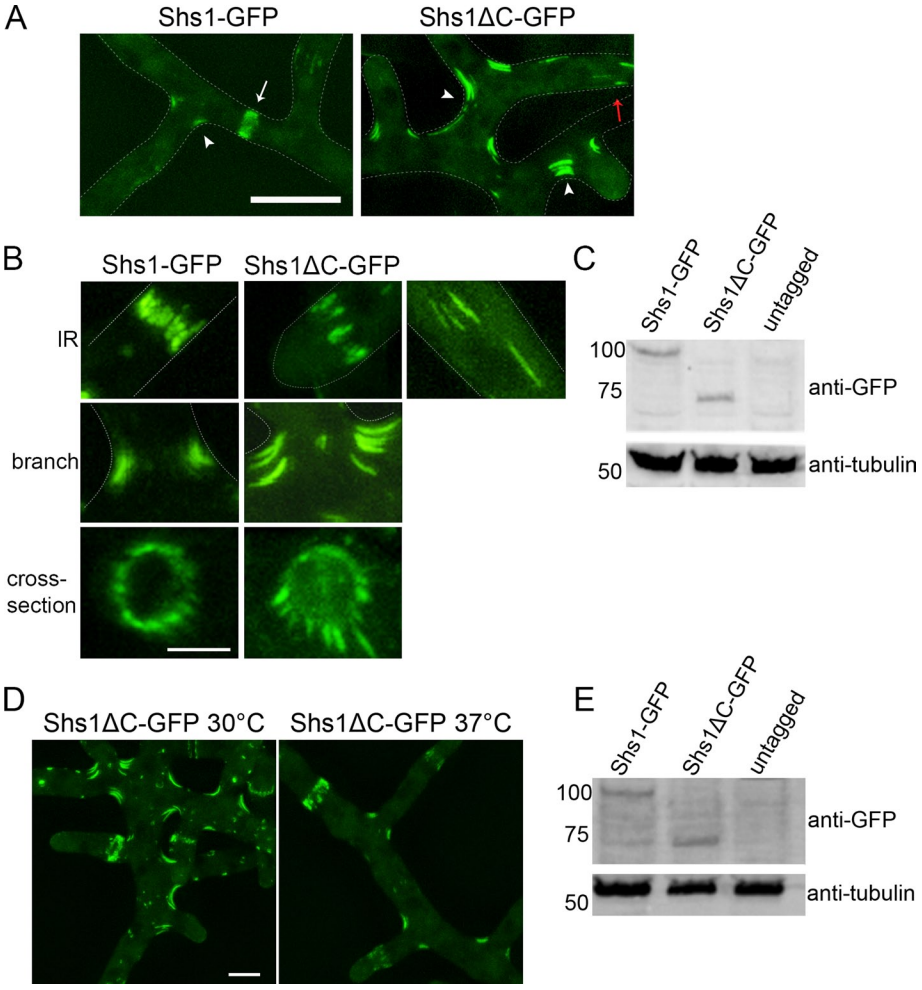

FIGURE 2: Loss of Shs1p C-terminus leads to an increased zone of septin ring assembly. (A) Loss of the Shs1p C-terminus leads to expanded branch rings and ectopic fiber formation throughout the IR. Cells expressing Shs1-GFP (AG124) and Shs1ΔC-GFP (AG539.2) were visualized by wide-field fluorescence microscopy. IR rings are indicated by white arrows and branch rings are indicated by white arrowheads. Ectopic fibers in the IR are indicated by a red arrow. Scale bar: 10 μm. (B) Zoomed-in view of IR and branch ring structures in Shs1-GFP compared with Shs1ΔC-GFP cells. Cell outlines are represented by dotted white lines. Scale bar: 2.5 μm. (C) Expression for Shs1ΔC is comparable with wild-type levels. *Ashbya* lysates for the indicated strains were separated on SDS–PAGE (10% acrylamide) and probed with anti-GFP antibody. Tubulin was used as a loading control. (D) Expanded rings are temperature sensitive. Shs1ΔC-GFP was grown overnight at 30°C or 37°C. Cells were imaged live by wide-field fluorescence microscopy. Scale bar: 10 μm. (E) Shs1ΔC-GFP is stably expressed at 37°C. *Ashbya* lysates for the indicated strains grown at 37°C were separated on SDS–PAGE (10% acrylamide) and probed with anti-GFP and anti–α-tubulin antibodies.

polarity. It is possible that the hyphal width defect arises in the mutant cells, because the concentration of Shs1p at the tips is substantially decreased (Figure 3E, quantified in Figure 6C later in the paper, $n > 100$ tips each; $p < 0.0001$). Overall, the C-terminus of Shs1p is required for normal recruitment of septin to hyphal tips, but not to septin rings, and leads to larger rings at branches and aberrant cell morphology.

Expansion of septin rings occurs at ring assembly in a kinase-independent manner

The size of a septin ring in normal *Ashbya* cells is determined at the birth of the ring and remains constant throughout the lifetime of the structure until septation is initiated many hours after ring assembly (DeMay *et al.*, 2009). The expanded septin rings and ectopic fibers seen in Shs1ΔC-GFP cells could arise during ring assembly such that newly assembled rings are abnormally large, which would suggest a defect in the initial scaling of the ring. Alternatively, the expanded zone of the septin ring could result from continued septin polymerization after the initial assembly, which would suggest a defect in limiting the window of assembly in both time and space. For determination of when the expanded septin rings form, Shs1ΔC-GFP–expressing cells were captured by time-lapse fluorescence microscopy. Frames from a representative movie (Supplemental Movie) shown in Figure 4A illustrate that the expanded zone of septin is present at the birth of the ring (arrow) and that the expanded rings persist over time but do not continue lengthening after the ring is initially built (arrowhead). Furthermore, additional fibers do not appear to form after establishment of the ring. Thus the C-terminus of Shs1p is required for setting the initial size of septin rings at the time of assembly.

It is not known what determines the length of a septin ring during assembly and what restricts its expansion along the cortex after that length has been reached. One possibility is that assembly is limited to a finite time period, and the final size is determined by the rate of septin polymerization in that time. If so, Shs1ΔC rings potentially are larger as there is simply more polymerization per unit time. To investigate whether Shs1ΔC promotes increased septin polymerization, we assessed whether these mutants were more sensitive to the septin-polymerizing small molecule forchlorfenuron (FCF). Treatment of *Ashbya* cells with FCF leads to extensive polymerization of septin-based fibers throughout the hyphae (DeMay *et al.*, 2010). We hypothesized that if Shs1ΔC-GFP promotes more rapid septin fiber formation, FCF-induced septin fibers would arise more quickly and/or at lower FCF concentrations. Cells were treated with 10, 25, 62.5, and 125 μM FCF for 30, 60, 90, and 120 min. No gross differences for the induction of septin fibers between wild-type and Shs1ΔC were apparent at any time or concentration of FCF (Figure 4B). This result suggests loss of the Shs1p C-terminus does not increase septin polymerization, or at least not in a way that is synergistic with FCF's mode of action.

We previously showed that the Elm1p and Gin4p kinases are required to assemble septin rings throughout the IR, although branch rings still form normally in those mutants (DeMay *et al.*, 2009). Despite the loss of all Shs1p phosphorylation sites in the Shs1ΔC mutant, septin rings are built normally throughout the IR of the cell, but with the addition of ectopic fibers in the IR that are not a component of a ring. We sought to test the role of the kinases in assembling expanded septin rings and ectopic fibers in the Shs1ΔC-GFP mutant by deleting the *ELM1* allele in the *shs1ΔC* background. Without Elm1p, IR rings are unable to form for both wild-type and

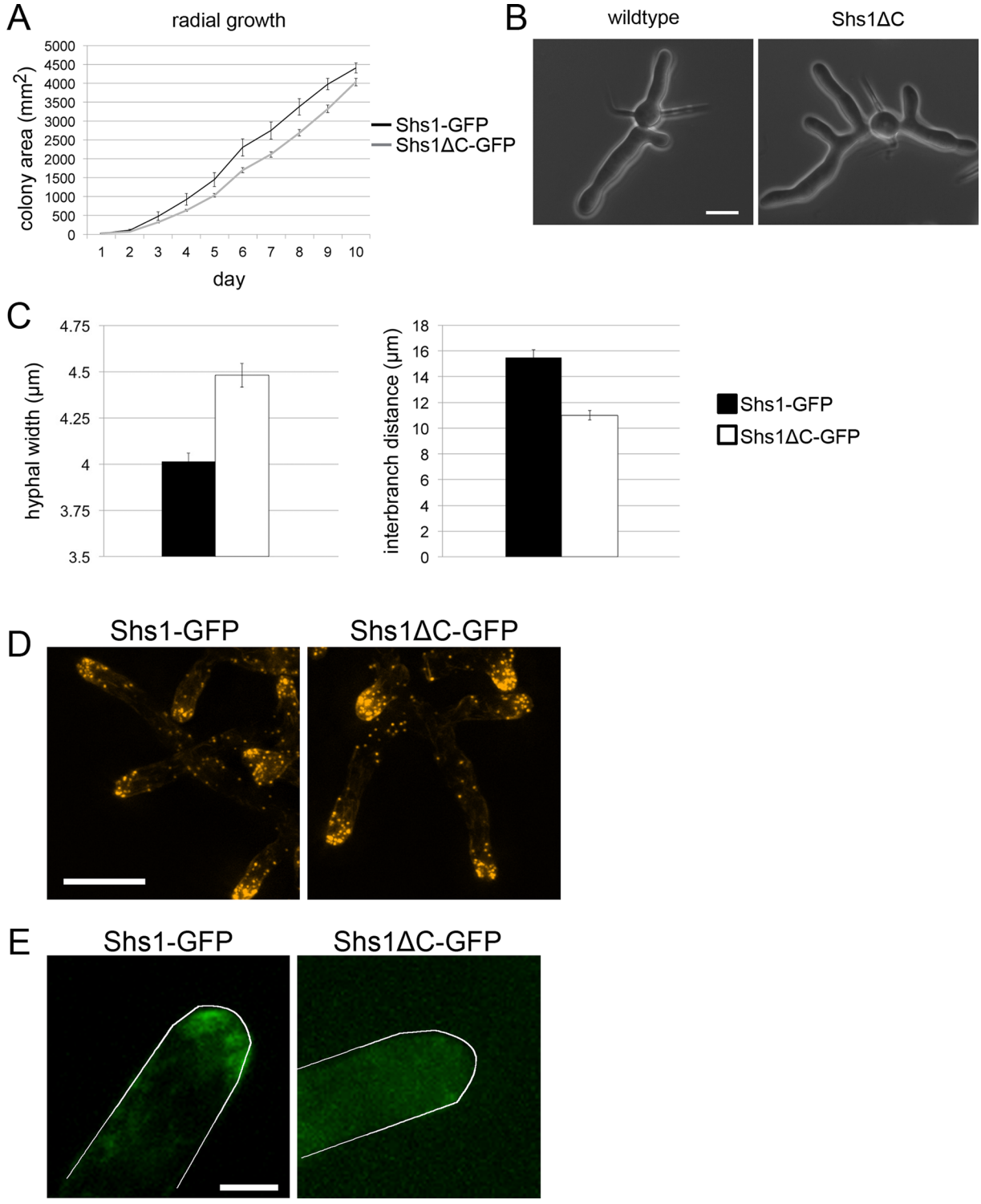

FIGURE 3: Loss of the Shs1p C-terminus causes cell morphological defects. (A) Shs1ΔC has a slight, but statistically significant, growth defect. Shs1-GFP (AG124) and Shs1ΔC-GFP (AG539.2) cells were grown on AFM G418 agar plates for 10 d ($n = 3$ each strain). Plates were imaged every 24 h, and colony growth was measured in area. Average slope for Shs1ΔC is 458.9 mm^2/d vs. 528.7 mm^2/d for Shs1-GFP ($p < 0.05$, determined with a two-tailed t test). (B) Shs1 C-terminal deletion leads to cell morphological defects. Phase-contrast images of Shs1-GFP and Shs1ΔC-GFP cells grown for 12 h are shown. Scale bar: 10 μm. (C) Hyphal width and interbranch distance are altered in the Shs1ΔC strain. Hyphal widths were measured for each hypha in cells grown for 14 h (left). $n \geq 196$ hyphae each ($p < 0.0001$, two-tailed t test). The length between branches was measured for cells cultured for 14 h (right). $n > 300$ interbranch distances for each strain ($p < 0.0001$, two-tailed t test). (D) Actin polarization is not altered in Shs1ΔC. Shs1-GFP and Shs1ΔC-GFP cells were grown overnight, fixed, and stained for actin. Actin patches polarized to several tips for each strain are shown. Scale bar: 10 μm. (E) Septin localization to the tips is defective in Shs1ΔC cells. Zoomed-in view of septin localization to the tips of cells expressing Shs1-GFP and Shs1ΔC-GFP. Scale bar: 2.5 μm.

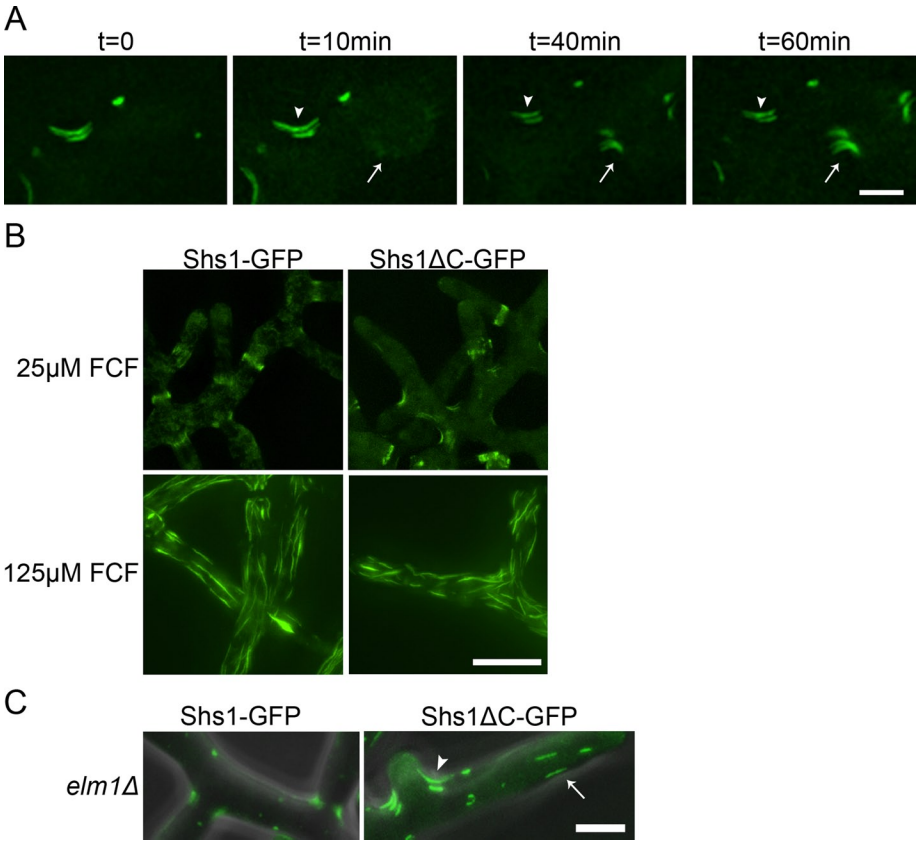

FIGURE 4: Septin ring assembly timing and FCF-induced fiber formation are unaffected by the loss of the Shs1 C-terminus. (A) Expanded branch ring size is established at assembly. Shs1ΔC-GFP (AG539.2) cells were imaged every 10 min for 1 h. A preexisting expanded branch ring is indicated by arrowheads. An emerging ring is indicated by arrows. Scale bar: 2.5 μm. (B) Polymerization of Shs1p by the small molecule FCF is unaltered in Shs1ΔC strain. Shs1-GFP and Shs1ΔC-GFP cells were grown 14 h at 30°C and were treated with various concentrations of FCF. Cells were sampled every 30 min for 2 h. Representative images after 2 h in the indicated concentration of FCF are shown. Scale bar: 10 μm. (C) Ectopic fiber formation does not require the Elm1p kinase. *elm1Δ* cells expressing Shs1-GFP (AG120) or Shs1ΔC-GFP (AG632.1) were imaged live. Ectopic fibers at the IR are indicated with an arrow, and an expanded branch ring is indicated with an arrowhead. Scale bar: 5 μm.

Shs1ΔC cells. However, the expanded branch rings and ectopic fibers in the IR in Shs1ΔC-GFP still form, despite the loss of the kinase (Figure 4C). This indicates Elm1p is not required for increasing the zone of septin structure formation.

Shs1ΔC-GFP interacts with other septin subunits

We hypothesized that loss of the C-terminus may be promoting homomeric Shs1 complex formation and that the expanded assemblies potentially are not composed of pure heteromeric septin filaments. Notably, however, Shs1ΔC-GFP can coimmunoprecipitate Cdc11p comparable with wild-type Shs1p (Figure 5A) and Shs1ΔC-GFP interacts with all four of the other septin subunits in a stoichiometric manner (Figure 5B). Additionally, we found that Cdc11 localizes to the elongated fibers both at the branch rings and throughout the IR, as detected by immunofluorescence, further indicating Shs1ΔC-GFP is not the only constituent of these expanded rings and aberrant filaments (Figure 5C). Thus Shs1ΔC-GFP is still able to efficiently interact with the other septins, indicating the C-terminus of Shs1 is dispensable for complex formation and excess septin structures seen in the mutant are not aberrant homomeric fibers. Intriguingly, Cdc11p is not concentrated at hyphal tips in the Shs1ΔC-GFP background (Figure 5D), suggesting that when Shs1p is not localizing normally to the tips, the other septins cannot concentrate there either. Therefore Shs1p oligomerizes with the other septins in this mutant, and deletion of the Shs1p C-terminus diminishes the ability of other septins to localize to the hyphal tips.

The coiled-coil of Shs1p is necessary for normal septin morphology

Because the C-terminus of Shs1p encompasses nine phosphorylation sites and a coiled-coil domain, either the phosphorylation sites or the coiled-coil domain could be responsible for regulating the formation of properly sized septin rings. Mutants expressing a nonphosphorylatable or phosphomimetic form of Shs1p (Shs1-GFP 9A or 9D, respectively) or Shs1p with the coiled-coil deleted (Shs1ΔCC-GFP, residues 459–508 deleted) were assessed for their ability to form septin rings (Figure 6A). The loss of the phosphorylation sites had no effect on the appearance of any of the septin rings (Figure 6B). The phosphomimetic Shs1-GFP 9D was dominant and lethal, so its effect on higher-order septin structure could not be assessed. Intriguingly, the loss of the Shs1p coiled-coil phenocopied the C-terminal truncation (Figure 6B). Shs1ΔCC-GFP localizes to a broader zone at branch rings and to ectopic fibers throughout the IR. We also assessed the mean fluorescence of Shs1p localizing to tips in these strains and found that, similar to Shs1ΔC-GFP, Shs1ΔCC-GFP is diminished at tips; however Shs1-GFP 9A recruitment to the tips is not significantly different from wild-type (Figure 6C, $n \geq 98$ for each strain). As for Shs1ΔC-GFP, the expanded branch rings and depletion of septins at tips are not a result of different expression of Shs1ΔCC-GFP compared with wild-type (Figure 6D). These data indicate the coiled-coil of Shs1p is playing an important role in septin ring geometry and scaling in *Ashbya*.

Shs1ΔCC-GFP alters septin mobility and concentration in rings

Septin rings are assembled at a fixed size in *Ashbya* but are able to incorporate new protein through time and are dynamic (DeMay *et al.*, 2009, 2010). It is not known whether septin dynamics contribute to scaling of septin rings in any system. Therefore we were interested to evaluate how loss of the Shs1p coiled-coil and/or phosphorylation may impact either the amount or rate of septin incorporation in rings or the stability of septin-based structures. To assess the relative amount of Shs1p incorporating into septin structures at steady state, we measured the fluorescence intensity of a region of fixed size for IR and branch rings, in Shs1ΔC-GFP, Shs1ΔCC-GFP, and Shs1-GFP 9A compared with Shs1-GFP (IR ring: $n \geq 80$ each strain; branch ring: $n \geq 48$ each strain). Mean fluorescence intensity at IR rings was significantly decreased

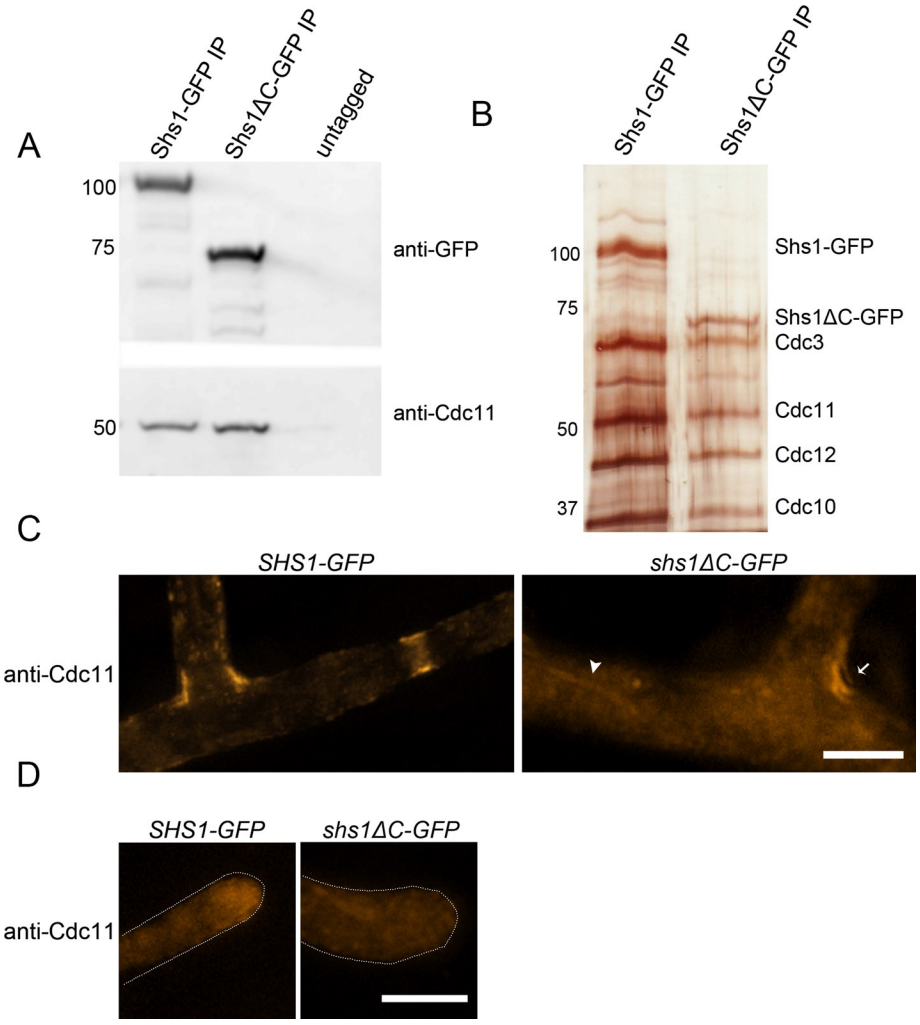

FIGURE 5: Shs1ΔC interacts with other septins. (A) Shs1ΔC-GFP interacts with Cdc11p. Shs1-GFP (AG124) and Shs1ΔC-GFP (AG539.2) were immunoprecipitated from *Ashbya* lysates using anti-GFP antibody. Immunoprecipitates were separated by SDS–PAGE, transferred to PVDF membrane, and probed with anti-GFP or anti-Cdc11 antibodies. (B) Shs1ΔC-GFP complexes with the other septins. Shs1-GFP and Shs1ΔC-GFP were immunoprecipitated from *Ashbya* lysates using anti-GFP antibody. Immunoprecipitates were separated by SDS–PAGE and silver-stained to assess coprecipitating proteins. (C) Shs1-GFP and Shs1ΔC-GFP cells were fixed with formaldehyde, spheroplasted with zymolyase, and probed with anti-Cdc11 antibody. An ectopic fiber in the IR is indicated with an arrowhead, and an expanded branch ring is indicated with an arrow. Scale bar: 5 μm. (D) Cdc11 localization is diminished at the tips in Shs1ΔC. Scale bar: 5 μm.

for Shs1ΔCC-GFP and significantly increased for Shs1-GFP 9A, compared with wild-type (Figure 7A; $p < 0.05$). This suggests the coiled-coil and phosphorylation of Shs1 are performing opposing roles in concentrating septin at the IR. The mean fluorescence intensities for branch rings in all mutant strains were comparable with wild-type (Figure 7B). Thus, despite the increase in the zone of septin assembled at branches, the concentration of septin in a given area of either ring type is unchanged. This indicates septins are recruited to a larger region at branch sites, but the amount of septin that gets recruited per unit area is the same in wild-type and Shs1 mutant cells.

The coiled-coil and/or phosphorylation of Shs1p could be responsible for regulating septin ring dynamics. It is easy to imagine that the melting and annealing of coiled-coil structures may be rate-limiting for dynamics or that phosphorylation induces structural changes that influence septin turnover. Potentially, altered dynamics could contribute to defects in ring scaling or changes in septin concentration. Entire septin rings in Shs1ΔC-GFP, Shs1ΔCC-GFP, and Shs1-GFP 9A cells were photobleached and fluorescence recovery was followed through time to test this ($n \geq 7$ rings for both ring types in all strains). No statistically significant change in mobile fraction or $t_{1/2}$ was observed for any of the mutant branch rings compared with wild-type, although there was a trend toward somewhat higher mobility in the coiled-coil mutants at branch rings. At the IR rings, Shs1-GFP 9A showed dynamics and mobile fraction similar to those of wild-type. However, the mobile fraction of Shs1ΔCC-GFP significantly increased (Table 1 and Figure 7C; $p < 0.05$). The relative $t_{1/2}$ of Shs1ΔCC-GFP recovery at IR rings is comparable with the wild-type $t_{1/2}$. However, the nearly doubled mobile fraction and this similar $t_{1/2}$ indicate that the absence of the coiled-coil increases the amount of Shs1p that can turn over and increases the actual rate of recovery by about twofold. This suggests the Shs1p coiled-coil normally limits septin dynamics, while phosphorylation has no significant effect on Shs1p dynamics in either ring type.

Shs1p may be turning over at the ring as a monomer or in complex with the other members of a heteromeric septin protofilaments. We hypothesized that the loss of the Shs1p coiled-coil may also increase the dynamics of other septins at the IR rings. Cdc11-mCherry was expressed in wild-type and Shs1ΔCC strains, and fluorescence recovery after photobleaching (FRAP) was monitored for Cdc11-mCherry at the IR rings to test this (Table 2 and Figure 7D). Regardless of the whether the Shs1p coiled-coil was present, there was no change in mobile fraction or $t_{1/2}$ of Cdc11-mCherry. These results indicate that the increased dynamics of Shs1ΔCC-GFP do not affect those of Cdc11p and provide evidence that the turnover of individual septin subunits may be regulated independently of other septins.

Ag Shs1ΔCC alters yeast septin ring and cell morphology

To test whether the Shs1p coiled-coil has a conserved function in regulating the geometry and scale of septin rings, we heterologously expressed *Ashbya gossypii* Shs1ΔC-GFP (*Ag* Shs1ΔC-GFP) in the budding yeast *Saccharomyces cerevisiae*. When expressed on a plasmid as the only copy of Shs1p (in an *shs1*Δ), *Ag* Shs1ΔC-GFP altered both cell and septin ring morphology in yeast (Figure 8A). The majority of cells expressing *Ag* Shs1ΔC-GFP as the sole form of Shs1p are elongated and have asymmetric septin rings. Although these yeast cells do not form ectopic fibers as in *Ashbya*, it is evident that Shs1ΔC has a striking effect on cell and septin ring shape. As in *Ashbya*, the mutant phenotype caused by Shs1ΔC is recessive, such

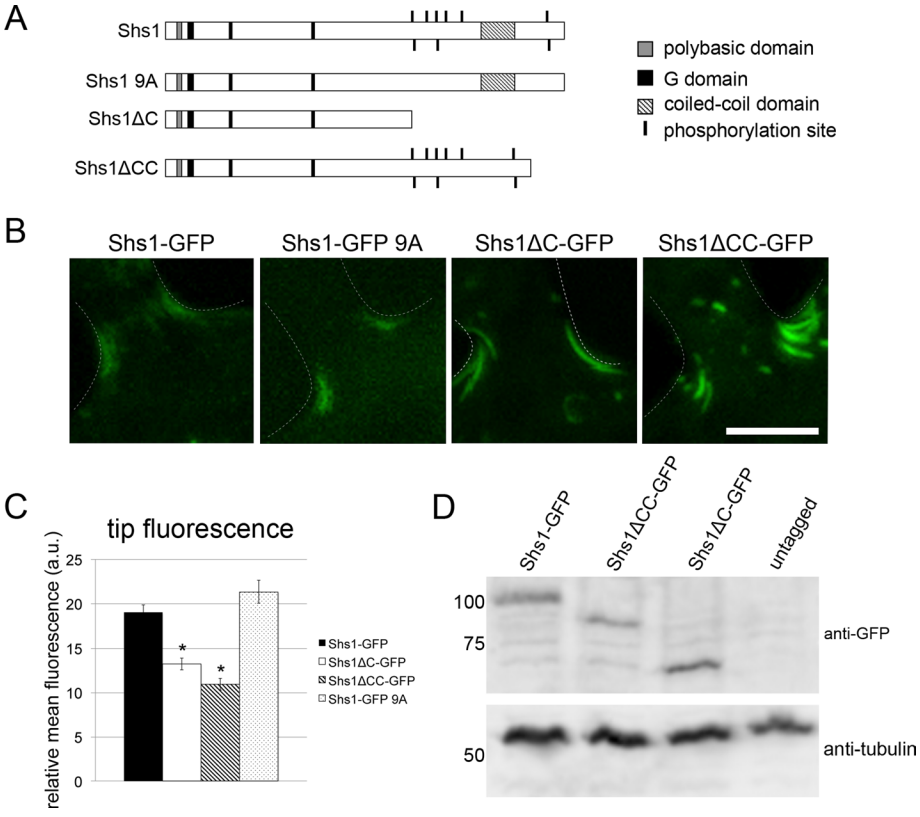

FIGURE 6: The coiled-coil of Shs1p, but not phosphorylation, is necessary for normal septin morphology. (A) Schematics for Shs1p mutants. (B) Deletion of the Shs1p coiled-coil produces expanded branch rings. Shs1-GFP (AG124), Shs1-GFP 9A (AG643.1), Shs1ΔC-GFP (AG539.2), and Shs1ΔCC-GFP (AG623) were grown for 14 h at 30°C and imaged live. Scale bar: 5 µm. (C) Quantification of septin fluorescence above cytosolic background levels at hyphal tips. Shs1-GFP, Shs1ΔC-GFP, Shs1ΔCC-GFP, and Shs1-GFP 9A cells were imaged on a wide-field fluorescence microscope, and images were contrasted to the same levels. Fluorescence intensities for a given volume of individual tips were measured using Volocity ($n \geq 98$ each). Cytosolic background was subtracted, and values for tips with a relative mean fluorescence above background are shown. Statistical significance was determined using a two-tailed *t* test, $*p < 0.0001$. Error bars represent SE. (D) Shs1ΔCC-GFP is expressed at levels comparable with those of Shs1-GFP. *Ashbya* lysates for the indicated strains grown at 30°C were separated on SDS–PAGE (10% acrylamide) and probed with anti-GFP and anti–α-tubulin antibodies.

that expressing *Ag* Shs1ΔC-GFP in a strain with the wild-type *S. cerevisiae SHS1* (*Sc SHS1*) allele produces cells with normal shape and septin rings (Figure 8B). The loss of the coiled-coil domain alone is sufficient to produce the aberrant cell and septin phenotypes seen in the Shs1p C-terminal deletion mutant. Expression of *Ag* Shs1ΔCC-GFP as the sole copy of Shs1p in yeast phenocopied Shs1ΔC and led to elongated cells and asymmetrical septin rings (Figure 8C). Deletion of the *Sc* Shs1 C-terminus (residues 470–551), including its predicted coiled-coil, displayed no apparent cell or septin defects (Figure S2), indicating the septin and cell size regulatory roles performed by the *Ashbya* Shs1p coiled-coil may not be shared by *S. cerevisiae* Shs1p.

DISCUSSION

The roles for the *Ashbya* Shs1p coiled-coil are summarized in Figure 9. In wild-type cells, septins localize to a cloud at the tip of growing hyphae and to rings of a fixed size at branches and in the IR. The deletion of the Shs1p coiled-coil leads to a loss of tip septin recruitment, increases the zone branch rings occupy, and causes ectopic fiber formation in the IR. Additionally, Shs1p lacking its coiled-coil is more mobile. Overall, the data we present in this paper are consistent with a role for the coiled-coil domain of Shs1p in limiting septin ring size and dynamics.

These results were surprising, considering that the coiled-coil is generally thought to enhance septin–septin interactions and facilitate oligomerization and filament formation. It is possible that the role in limiting size and dynamics of septin rings is particular to the coiled-coil of Shs1p. Of the five septins in *Ashbya* and *S. cerevisiae*, Shs1p remains the most mysterious. It is nonstoichiometric in both organisms, although it is substoichiometric in yeast and superstoichiometric in *Ashbya* based on fluorescence intensities at rings (Mortensen *et al.*, 2002; DeMay *et al.*, 2009). It has been proposed that Shs1p is an accessory septin that can substitute for Cdc11p at the terminal position in the hetero-octamer (Garcia *et al.*, 2011). In vitro complexes formed by purified septins from *Ashbya* are hetero-octamers, suggesting that only four of the five septins are present in any given heteromer. Thus, in *Ashbya*, the complexes that are immunoprecipitated from lysates are either polar protofilaments with Cdc11p and Shs1p at opposite ends or are nonpolar decamers in which the capping septin has a weaker association with the complex than the underlying octamer and can fall apart after the initial immunoprecipitation step, before visualization with electron microscopy. The salt concentration of the immunoprecipitation buffer is sufficiently high that it is unlikely a single Shs1 molecule is pulling out multiple protofilaments. The existence of polar protofilaments is an intriguing possibility, because it would suggest septin polymers are nonpolar when an even number of different subunits are available, but can potentially form polar filaments when given an odd number of different subunits. This has important ramifications for septin polymerization in mammalian cells, in which many different septins and isoforms are coexpressed.

When recombinant yeast septin complexes containing Shs1p in place of Cdc11p are incubated in a low-salt solution that normally promotes long, straight filament formation, the complexes self-assemble into rings (Garcia *et al.*, 2011). This suggests Shs1p is capable of promoting curvature to septin assemblies. Given that septin higher-order complexes are found in highly curved areas, such as the yeast mother-bud neck, the branch sites of *Ashbya*, and the bases of dendritic spines in neurons, it makes sense that the septin complex would have intrinsic curvature. In vitro, the C-terminus of yeast Shs1p is required for the septin complexes to self-assemble into rings, but it is not required for oligomerization into complexes (Garcia *et al.*, 2011). These special features of the *S. cerevisiae* Shs1p and the requirement for the C-terminus, which includes a predicted coiled-coil domain, suggest that Shs1p has the potential to play important roles in septin ring organization in the cell and may react to and/or generate membrane curvature.

Because the loss of the Shs1p coiled-coil domain in *Ashbya* leads to an expansion of septin branch rings and a loss of septin

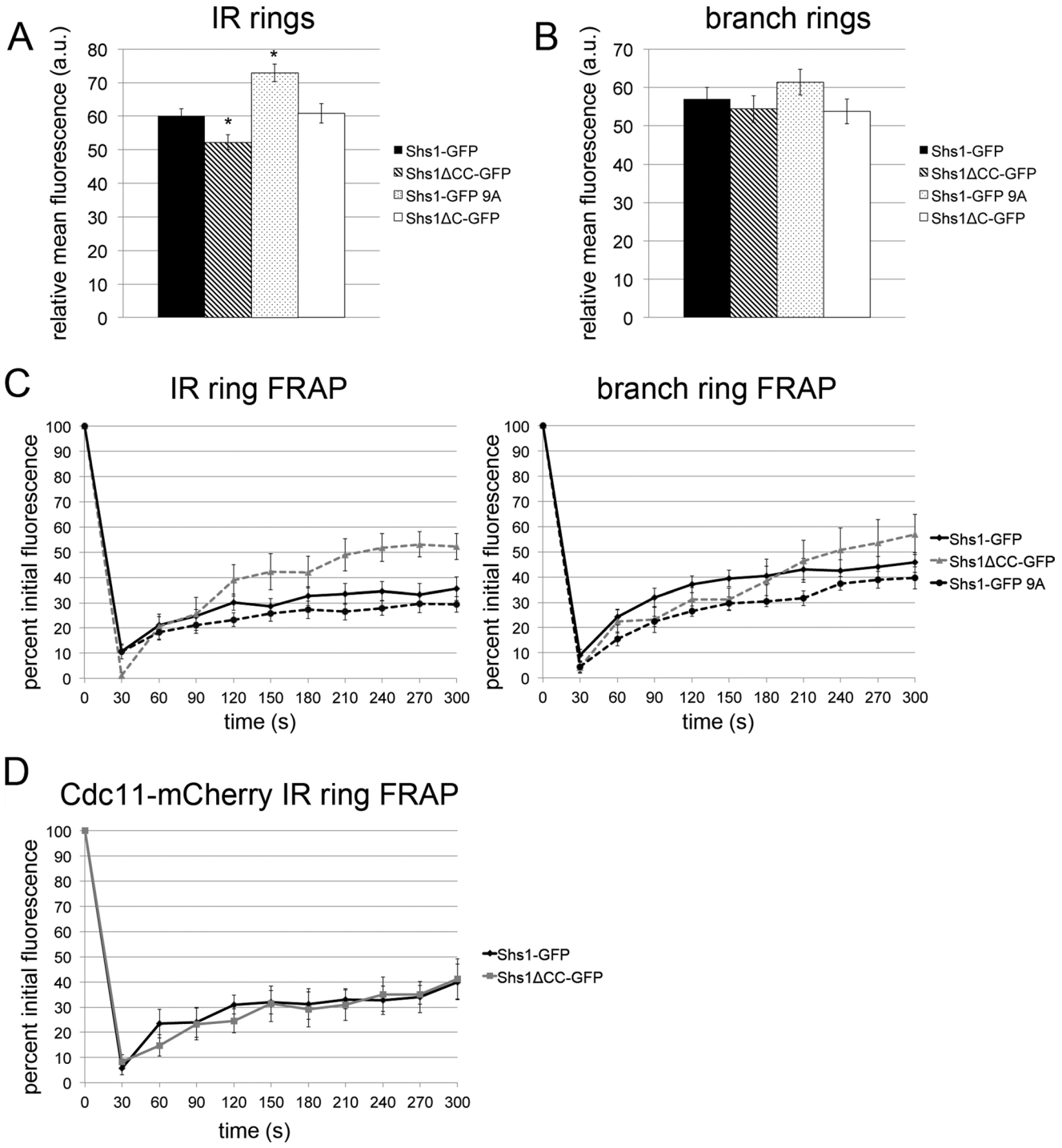

FIGURE 7: Shs1ΔC-GFP alters higher-order structure dynamics. (A) Concentration of Shs1ΔCC in IR rings is increased and Shs1 9A is decreased compared with wild-type levels. Shs1-GFP (AG124), Shs1ΔCC-GFP (AG623), Shs1-GFP 9A (AG643.1), and Shs1ΔC-GFP (AG539.2) cells were imaged on a wide-field fluorescence microscope, and images were contrasted to the same levels. Fluorescence intensities for a given volume of individual rings were measured ($n \geq 80$ for each strain). Cytoplasmic background was subtracted. Error bars represent SE, $^*p < 0.05$. (B) Concentration of Shs1 is unaltered in branch rings, regardless of mutations. Images and measurements were performed as described for A ($n \geq 48$ for each strain). (C) Shs1ΔCC-GFP is more mobile than wild-type Shs1-GFP in the IR rings. Shs1-GFP, Shs1ΔCC-GFP, Shs1-GFP 9A, and Shs1ΔC-GFP were imaged using confocal spinning-disk microscopy. Individual rings in each strain were bleached and then imaged every 30 s for 5 min ($n \geq 7$ rings per type). Fluorescence intensity of the bleached region was recorded at each time point. Intensities were corrected for cytoplasmic background and photobleaching. Error bars on the recovery curves represent SE. Statistical significance for mobile fraction and $t_{1/2}$ were determined by two-tailed *t* tests (Table 1). (D) Cdc11-mCherry dynamics are unchanged despite the loss of the Shs1 coiled-coil. FRAP was performed on Cdc11-mCherry in either a wild-type Shs1 (AG208) or Shs1ΔCC (AG664.1) background, as described for C ($n = 9$ IR rings for each strain). Summary statistics are presented in Table 2.

Ring type	n	Mobile fraction ± SD (%)	$t_{1/2}$ ± SD (s)
Shs1-GFP IR	14	32.2 ± 13.9	43.8 ± 10.4
Shs1ΔCC-GFP IR	8	60.9 ± 10.0[a]	41.4 ± 6.7
Shs1-GFP 9A IR	10	23.5 ± 6.9	51.6 ± 16.3
Shs1ΔC-GFP IR	7	47.5 ± 18.3[b]	31.8 ± 10.9
Shs1-GFP branch	20	45.5 ± 19.1	39.4 ± 13.9
Shs1ΔCC-GFP branch	8	57.4 ± 24.4	41.3 ± 10.4
Shs1-GFP 9A branch	10	39.4 ± 16.6	46.8 ± 8.1
Shs1ΔC-GFP branch	7	56.2 ± 27.5	42.1 ± 8.1

[a] $p < 0.05$ (analysis of variance).
[b] $p < 0.1$.

TABLE 1: Shs1 FRAP summary statistics.

localization to the hyphal tips, it is tempting to speculate that membrane curvature has a role for directing septin higher-order structure organization. Shs1ΔCC-GFP localizes more readily to branch sites than to tips, which suggests that in the absence of the Shs1p coiled-coil, septin complexes or filaments may be more easily recruited to convex rather than concave membrane surfaces inside the cell. The coiled-coil may be required for capping filaments or influencing septin complex curvature, such that it limits how far septin rings can expand along the membrane. Shs1p coiled-coil interactions with the membrane may depend on membrane composition. We speculate that the branch sites of *Ashbya* may have a different membrane lipid or protein composition than the membrane at the hyphal tips. Wild-type Shs1p, in this case, would have a higher affinity for specific lipids in the membrane at the tips than the Shs1p coiled-coil deletion. The decrease of ectopic fibers and branch ring expansion in the coiled-coil mutant at high temperatures may be consistent with an alteration in membrane composition or fluidity.

The association of septins with the cell cortex is still a very poorly understood facet of septin organization. It is clear that septins can interact directly with static lipids in vitro and the polybasic domain may contribute to this interaction, but additional surfaces, and in particular Cdc10p, may be critical for membrane bilayer association (Casamayor and Snyder, 2003; Bertin *et al.*, 2010). Additional in vitro data demonstrate that purified septins can self-assemble into filaments and orthogonal arrays when incubated with a PIP_2-1,2-dioleoyl-*sn*-glycero-3-phosphocholine (DOPC) lipid monolayer and that arrangement into orthogonal arrays, but not filament formation, under these conditions relies on septin coiled-coil domains (Bertin *et al.*, 2010). This suggests that formation of more elaborate septin assemblies are facilitated by membranes in a way that involves the septin coiled-coils, though it is not clear whether the coiled-coils can directly interact with the membranes. How septin interactions with the membrane are regulated in the cell remains an interesting open question.

Background	n	Mobile fraction ± SD (%)	$t_{1/2}$ ± SD (s)
Shs1-GFP	9	44.7 ± 15.6	40.9 ± 12.0
Shs1ΔCC-GFP	9	40.2 ± 23.1	41.9 ± 14.0

No statistically significant differences were observed (two-tailed *t* test).

TABLE 2: Cdc11-mCherry IR ring FRAP summary statistics.

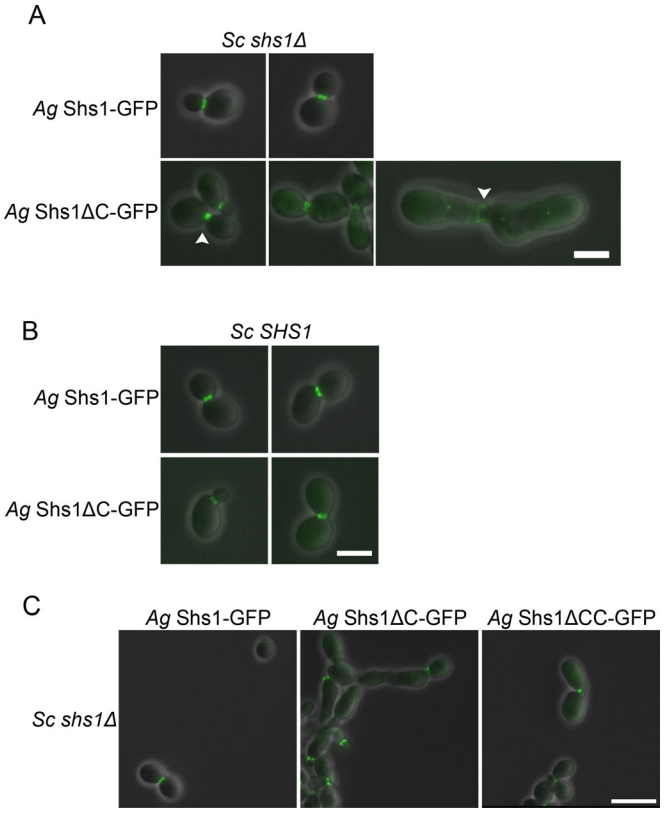

FIGURE 8: *Ashbya* Shs1ΔCC-GFP expression leads to aberrant cell and septin ring morphology in yeast. (A) *Ashbya* Shs1ΔC expressed as the only copy of Shs1p in the cell leads to yeast cell and septin defects. *S. cerevisiae shs1Δ* cells heterologously expressing plasmidic *A. gossypii* Shs1-GFP or Shs1ΔC-GFP were grown to log phase and imaged live. Arrowheads indicate misshapen septin rings at the mother-bud neck. Scale bar: 5 μm. (B) Shs1ΔC cell and septin morphology defects are recessive in yeast. *S. cerevisiae* cells with a wild-type copy of *SHS1* heterologously expressing plasmidic *A. gossypii* Shs1-GFP or Shs1ΔC-GFP were grown to log phase and imaged live. Scale bar: 5 μm. (C) *Ashbya* Shs1ΔCC-GFP expressed as the only copy of Shs1p in yeast produces defective cell and septin morphology in yeast. *S. cerevisiae* cells expressing *A. gossypii* Shs1-GFP, Shs1ΔC-GFP, or Shs1ΔCC-GFP on a plasmid were grown to log phase and imaged live. Scale bar: 5 μm.

The *Ashbya* Shs1p coiled-coil deletion leads to an increase in hyphal width and branching frequency, consistent with increased branching phenotypes seen in other filamentous fungal cells lacking coiled-coil domain-containing septins (Alvarez-Tabares and Perez-Martin, 2010; Lindsey *et al.*, 2010; Hernandez-Rodriguez *et al.*, 2012). This suggests that the mutant septin complexes themselves may play a role in promoting polarized growth throughout the hyphae, perhaps due to increased septin recruitment to the cortex at future branch sites. It is possible that the expanded area of septin localization can act as a scaffold to concentrate polarity machinery, leading to more hyphal branching.

We were intrigued to find that phosphorylation of Shs1p is not required for septin organization into rings, and in fact nonphosphorylatable Shs1-GFP 9A is significantly more concentrated at IR rings than wild-type Shs1-GFP. Localization to tips and branch rings, however, appears normal, and there is no change in Shs1p dynamics in this mutant. There are likely functional consequences of Shs1p phosphorylation, because mutating all Shs1p phosphorylation sites

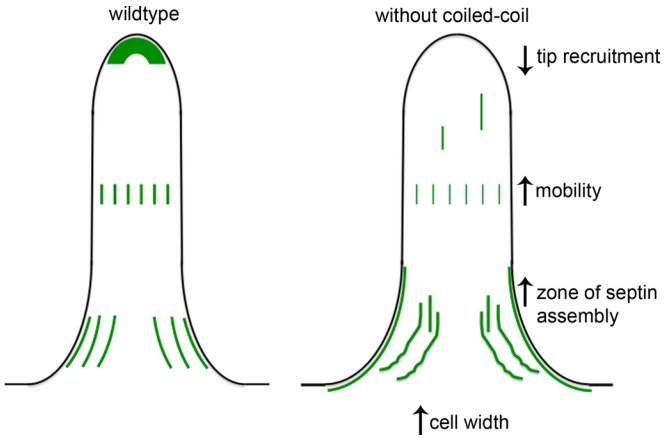

FIGURE 9: Summary of limitation of septin ring size and mobility by the Shs1p coiled-coil. Loss of the Shs1p coiled-coil leads to wider hyphae, enlarged septin rings at branches, ectopic fibers throughout the IR, and increased Shs1p mobility at the IR rings.

to the phosphomimetic residue aspartic acid was lethal. It has been established in *S. cerevisiae* and *Candida albicans* that the kinase Gin4p directly phosphorylates septins (Mortensen *et al.*, 2002; Sinha *et al.*, 2007), and loss of Gin4p activity leads to defects in septin ring formation and dynamics (Longtine *et al.*, 1998; Wightman *et al.*, 2004; Li *et al.*, 2012). We previously showed that the Elm1p and Gin4p kinases are required for septin ring formation in *Ashbya* (DeMay *et al.*, 2009). Because the cells with nonphosphorylatable Shs1p did not mimic the kinase mutant phenotype, the kinases must have other targets. It remains possible that *Ashbya* Shs1p is phosphorylated by Elm1p or Gin4p, but because additional targets—perhaps other septins—also get phosphorylated, simply the loss of Shs1p phosphorylation sites is not sufficient to cause a defect in ring assembly. Interestingly, in Shs1ΔC cells lacking Elm1p, ectopic fiber formation remains intact, although the normal IR rings are not able to assemble. This indicates that not all septin structure formation in the IR is reliant on Elm1p kinase activity. Again, we speculate that increased interaction of septins with the membrane in the mutant may be sufficient to overcome the need for phosphorylation.

The increased recovery after photobleaching of Shs1ΔCC compared with wild-type Shs1p indicates that in addition to limiting septin ring size, the Shs1p coiled-coil also limits the dynamics. The increased dynamics and increased ring size may be two distinct properties of the mutant protein or an indication that dynamics contribute to ring scaling. Approximately twice the amount of Shs1ΔCC can recover to IR rings in the same amount of time as its wild-type counterpart. It is possible, given the decreased steady-state concentration of Shs1ΔCC compared with wild-type, that individual bars comprising IR rings made of bundles of septins are thinner from membrane to cytoplasm, and the percent of septin exposed to the cytoplasm is therefore higher than it would normally be. This could result in the increased mobile fraction we observe for this mutant. Alternatively, the increased turnover could simply be a result of removing a dynamics-limiting property of the Shs1p coiled-coil. In *C. albicans*, it has been shown that Cdc10p, a septin that does not have a coiled-coil domain, is dynamic in hyphal septin rings, while other septins at the same location are not (Gonzalez-Novo *et al.*, 2008), suggesting septin coiled-coil domains may inhibit dynamics in other systems. Similarly, we demonstrate that the loss of the Shs1p coiled-coil increases the dynamics of Shs1p, but this mutation does not affect the dynamics of Cdc11p, whose coiled-coil remains intact. It is possible that melting and annealing of the coiled-coils is rate-limiting for septin turnover or that the coiled-coil restricts incorporation into the rings by forcing the subunits to be in a certain conformation for entry to or exit from the polymer. Much still remains to be known about how septin dynamics are regulated in any cell type, but we show here that the septin coiled-coils have the potential to contribute to regulation of septin turnover at higher-order assemblies. It will be interesting to test whether this is specific to the Shs1p coiled-coil, or whether this is a conserved function among other septins.

The data we present in this paper demonstrate a novel role for septin coiled-coils in directing septin higher-order structure scaling and dynamics. How the coiled-coil is functioning specifically—whether it is modulating septin–septin interactions, septin–membrane interactions, or interactions of septins with other proteins—remains to be uncovered. This work is an important first step in understanding how septin ring size and dynamics may be controlled by individual septin proteins.

MATERIALS AND METHODS

Growth conditions and strain construction

A. gossypii media, culturing, and transformation protocols have been described previously (Ayad-Durieux *et al.*, 2000; Wendland *et al.*, 2000). Strains generated and used in this study can be found in Table 3. AG442.1 was obtained by transforming Δ*l*Δ*t* cells with AGB088. To obtain AG495.1, we amplified *TAP-GEN3* from AGB275 using AGO649/650, and the PCR product was used to directly tag *CDC11A*. The strain was verified using primer pairs AGO653/654 and AGO651/652. AG539.2 was constructed using

Strain	Relevant genotype[a]	Source
wild-type	Δ*leu2*Δ*thr4*	Altmann-Johl and Philippsen, 1996
AG120	Ag*elm1*Δ::GEN3/Ag*SHS1-GFP-NAT1*	DeMay *et al.*, 2009
AG124	Ag*SHS1-GFP-GEN3*	Helfer and Gladfelter, 2006
AG208	pAGB141 [pAg *CDC11a-mCHERRY-NAT1*]/Ag*SEP7-GFP-GEN3*	This study
AG442.1	pAGB088 [pAg*SHS1-GFP-Gen*]	This study
AG495.1	Ag*CDC11a-TAP-GEN3*	This study
AG539.2	Ag*SHS1*Δ*C-GFP-GEN3*	This study
AG623	Ag*SHS1*Δ*CC-GFP-GEN3*	This study
AG632.1	Ag*elm1*Δ*nat*/Ag*SHS1*Δ*C-GFP-GEN3*	This study
AG643.1	Ag*SHS1-GFP-GEN3 9A*	This study
AG647.1	pAGB412.1 [pAg*SHS1*Δ*C-GFP-GEN3*]	This study
AG664.1	pAGB141 [pAg *CDC11a-mCHERRY-NAT1*]/Ag*SHS1*Δ*CC-GFP-GEN3*	This study

[a]With the exception of plasmidic strains (in brackets), all analyzed mycelia were homokaryotic (all nuclei have the same genotype).

TABLE 3: *Ashbya* strains used in this study.

direct integration of *GFP-GEN3* (amplified from AGB005 using AGO996/997) immediately upstream of the bases encoding Ser-359 in *SHS1*. The same PCR product was used to create AGB412.1 via gap repair of AGB088 cut with *Aat*II and *Bam*HI HF. The entire open reading frame (ORF) of the plasmid was sequence-verified using AGO5, 557, and 593. AG647.1 was created by transforming Δ*l*Δ*t* cells with the AGB412.1. AGB405 was constructed via overlap-extension PCR. Regions neighboring, but not including, the Shs1 coiled-coil were amplified using primer pairs AGO1061/1063 and AGO1062/5. The overlap-extension product was made using the products of the previous reactions and AGO1061/5. AGB88 was cut with *Aat*II and *Bam*HI HF, and this cut plasmid was gap-repaired via yeast cotransformation with the overlap-extension product. The final Shs1 coiled-coil deletion plasmid was confirmed by a test digest with *Apa*I and sequencing across the entire ORF with AGO5, 521, 557, 593, 684, and 1063. For integration into Δ*l*Δ*t*, AGB405 was cut with *Apa*LI and transformed into cells. The strain (AG623) was verified with primer pairs AGO365/520 and AGO428/5. AG632.1 was created by transforming AG539.2 cells with PCR product amplified from AGB009 with AGO452/453. The deletion was verified with primer pairs AGO26/235, AGO234/27, and AGO28/27. A gene encoding *SHS1 9A* (the nine phosphorylation sites changed to nonphosphorylatable alanine) was synthesized by Genscript (Piscataway, NJ) and contained in the pUC57 vector (AGB358). *SHS1 9A* was cut from the vector using *Sac*I and subcloned into pRS416, also digested with *Sac*I (AGB404). *GFP-GEN* was amplified from AGB005 using AGO953/AGO775 and cotransformed in yeast with AGB404 to yield AGB406. AGB406 was verified by test digests with *Eag*I and sequencing across the entire ORF with oligos AGO428, 520, 521, 557, 595, and 684. For integration into Δ*l*Δ*t*, the plasmid was digested with *Sap*I and transformed into cells. The resulting strain (AG643.1) was verified using primer pairs AGO365/520 and AGO557/684, as well as sequencing using AGO428. A similar cloning strategy was used for *SHS1 9D*. In short, a gene encoding *SHS1 9D* (the phosphorylation sites changed to phosphomimetic aspartic acid) was synthesized by Genscript in the pUC57 vector (AGB359). *SHS1 9D* was cut from pUC57 with *Sac*I and subcloned into pRS416 (AGB373). *GFP-GEN* was amplified from AGB005 using AGO953/AGO776 and cotransformed in yeast with AGB373 to yield AGB378. The entire ORF was sequenced as for AGB406. Strains AG208 and AG664.1 were obtained by transforming AG124 and AG623, respectively, with pCdc11a-mCherry-Nat (AGB141).

S. cerevisiae was grown overnight in yeast–peptone–dextrose media, plus 200 μg/ml G418 for GEN3 selection, if applicable. Yeast strains generated and used in this study can be found in Table 4. Yeast lacking a copy of *SHS1* were transformed with AGB088, AGB412.1, and AGB405 to yield AGY50, 51, and 52, respectively. Wild-type yeast (DHD5) were transformed with AGB088, AGB412.1, and AGB405 to yield AGY53, 54, and 55, respectively. The C-terminus of *S. cerevisiae SHS1* was truncated with a GFP-GEN cassette amplified from AGB005 using AGO1129/1130. The strain was confirmed via fluorescence microscopy.

Plasmids used in this study are listed in Table 5. PCR was performed using standard methods with polymerases from Roche Diagnostics (Indianapolis, IN) and Invitrogen (Carlsbad, CA). Oligonucleotides were synthesized by Integrated DNA Technologies (Coralville, IA), and all restriction enzymes came from New England Biolabs (Beverly, MA). Oligonucleotide primers are listed in Table 6. Plasmid isolation from yeast and sequencing were performed as described in Schmitz *et al*. (2006). All sequencing was performed by Dartmouth College Core Facilities (Hanover, NH).

Strain	Relevant genotype[a]	Source
DHD5 (wt)	*MATa/MATa ura3-52/ura3-52 leu2-3112/leu2-3112 his3-11,15/his3-11,15*	Schmitz *et al.*, 2006
AGY032	*MATa shs1Δtrp*	Erfei Bi, University of Pennsylvania, Philadelphia, PA
AGY50	pAGB088 [pAg *SHS1-GFP-GEN3*]//AGY032	This study
AGY51	pAGB412.1 [pAg *SHS1ΔC-GFP-GEN3*]//AGY032	This study
AGY52	pAGB405 [pAg *SHS1ΔCC-GFP-GEN3*]//AGY032	This study
AGY53	pAGB088 [pAg SHS1-GFP-Gen]// DHD5	This study
AGY54	pAGB412.1 [pAg *SHS1ΔC-GFP*-GEN3]//DHD5	This study
AGY55	pAGB405 [pAg *SHS1ΔCC-GFP-GEN3*]//DHD5	This study
AGY59	Sc *SHS1ΔC-GFP-GEN3*// DHD5	This study

[a]Brackets indicate expression from a plasmid.

TABLE 4: Yeast strains used in this study.

Radial growth assays were performed as previously described (Anker and Gladfelter, 2011).

Microscope setup and image processing

A Zeiss Axioimage-M1 upright light microscope (Carl Zeiss, Jena, Germany) equipped with a Plan-Apochromat 63×/1.4 numerical aperture (NA) oil objective was used for wide-field fluorescence microscopy. GFP signal was visualized with a Zeiss 38HE filter set and Alexa Flour 568 signal was visualized with Chroma filter set 41002B. An Exfo X-Cite 120 lamp was used as the fluorescent light source. Images were acquired on an Orca-AG charge-coupled device (CCD) camera (C4742-80-12AG; Hamamatsu, Bridgewater, NJ) driven by Volocity 5 (Perkin Elmer-Cetus, Waltham, MA). Live and immunofluorescence images were taken at 0.5-μm steps to encompass the depth of the entire hypha and were fast-deconvolved in Volocity 4. For live images used to ascertain the fluorescence intensity of a given area, 0.5-μm steps were taken over a total thickness of 9 μm. Time-lapse movies were acquired at a time interval of 10 min and iteratively deconvolved (45 iterations, Volocity 4).

Confocal time-lapse movies were acquired using a Yokogawa spinning-disk attached to a Nikon (Melville, NY) Eclipse Ti utilizing a Nikon 100×/1.4 NA Plan-Apo VC objective, controlled by MetaMorph 7 (Molecular Devices, Sunnyvale, CA). This system was assembled by Quorum Technologies (Guelph, Ontario, Canada). Photobleaching of entire septin rings was performed using a 405-nm laser at 70% power (1000-ms, 450-mW laser) in conjunction with a Mosaic micromirror array system. Images were captured using a Hamamatsu ImagEM C9100-13 electron multiplying (EM)-CCD camera. GFP was imaged using 30% laser power (491-nm laser) exposed for 200 ms/slice. mCherry was imaged using 30% laser power (561-nm laser) exposed for 250 ms/slice. Seventeen-slice Z-stacks (0.5-μm steps) through the entire hypha were imaged at 30-s intervals.

Live cells (*Ashbya* and yeast) were imaged on 2% agarose gel pads made with 2× low-fluorescence minimal media, covered with a

Number	Name	Vector	Relevant insert	Source
	pRS416			Sikorski and Hieter, 1989
AGB005	pAGT141	pUC19	*GFP-GEN3*	Kaufmann, 2009
AGB009	pAGT100	pUC19	*NAT1*	Kaufmann, 2009
AGB088	pAgShs1-GFP-Gen	pRS416	*SHS1-GFP-GEN3*	Helfer and Gladfelter, 2006
AGB141	pAg Cdc11a-mCherry-Nat	pRS416	*CDC11a-mCHERRY-NAT1*	DeMay *et al.*, 2009
AGB275	pTAP-Gen	pUC19	*TAP-GEN*	Peter Philippsen, University of Basel, Switzerland
AGB358	pAg Shs1 9A	pUC57	*SHS1 9A*	This study
AGB359	pAg Shs1 9D	pUC57	*SHS1 9D*	This study
AGB373	pAg Shs1 9D pRS416	pRS416	*SHS1 9D*	This study
AGB378	pAg Shs1-GFP-Gen 9D	pRS416	*SHS1-GFP-GEN3 9D*	This study
AGB404	pAg Shs1-GFP 9A	pRS416	*SHS1-GFP 9A*	This study
AGB405	pAg Shs1ΔCC-GFP-Gen	pRS416	*SHS1ΔCC-GFP-GEN3*	This study
AGB406	pAg Shs1-GFP-Gen 9A	pRS416	*SHS1-GFP-GEN3 9A*	This study
AGB412.1	pAg Shs1ΔC-GFP-Gen	pRS416	*SHS1ΔC-GFP-GEN3*	This study

TABLE 5: Plasmids used in this study.

glass coverslip, and sealed with lanolin or Vaseline–lanolin–paraffin. All images and movies (wide-field and confocal) presented here are maximum projections of three-dimensional volumes.

Fluorescence intensity and FRAP analysis

All fluorescence intensity and FRAP measurements were taken in Volocity 4.

Mean fluorescence intensity measurements for septin rings and septin clouds at hyphal tips were measured using a region of interest of the same area for each structure type. Cytosolic background was measured by subtracting an average of five background mean fluorescence measurements in the same cell as the measured ring from the mean fluorescence intensity of the ring.

To measure the intensity of a given ring over the course of a FRAP movie, we drew a region of interest around the entire ring, and the mean fluorescence value per pixel of the selected area was recorded. An adjacent region of cytosol was measured, and this mean fluorescence value was subtracted from the mean fluorescence of the ring to yield the mean fluorescence of the ring minus the background. Photobleaching was corrected for by using the mean fluorescence intensity of a ring of the same type in the same field. The regions of interest around the rings were shifted as necessary to compensate for cell drift during the movie. The mobile fractions for each ring were calculated by dividing percent recovery by percent bleach, and mobile fractions were averaged to obtain the average mobile fractions and SDs listed in Tables 1 and 2. The $t_{1/2}$ for each ring was calculated using the formula $t_{1/2} = t_{maxfl} \times (\log(0.5)/\log(1/\text{mobile fraction})$, where t_{maxfl} is the time point at which recovery plateaus. Average $t_{1/2}$ and SD values are listed in Tables 1 and 2. Statistical significance of the mobile fraction and $t_{1/2}$ measurements were determined by two-tailed *t* tests.

FCF treatment

FCF (Sigma-Aldrich, St. Louis, MO) was dissolved in 99.5% ethanol to a stock concentration of 250 mM. The stock was diluted directly in the liquid media of cell cultures grown overnight for 14 h to bring FCF to a final concentration of 25–125 μM. After addition of FCF, cells were incubated at growth conditions for an additional 30–120 min. Treated cells were fixed for 10 min in 2% paraformaldehyde (Sigma-Aldrich) to preserve GFP signal. Cells were washed twice in 1× PBS and resuspended in ProLong Gold antifade reagent (Invitrogen).

Immunofluorescence

Immunofluorescence was performed as described previously (Gladfelter *et al.*, 2006). Rabbit anti-ScCdc11p (Santa Cruz Biotechnology, Santa Cruz, CA) was diluted in 1× PBS + 1 mg/ml bovine serum albumin and used at a 1/50 dilution. Cells were incubated with primary antibody overnight at 4°C. Primary antibody was detected and visualized using Alexa Fluor 568 anti-rabbit (Invitrogen) at a 1/200 dilution.

Visualization of F-actin

For viewing F-actin, cells were fixed with 3.7% formaldehyde (Fisher Scientific, Fair Lawn, NJ) at 30°C for 1 h. Cells were washed twice in 1× phosphate-buffered saline (PBS) and resuspended in 1× PBS. Cells were incubated with Alexa Fluor 568 phalloidin (Invitrogen) at a final concentration of 6.6 μM for 1 h at room temperature in the dark. Cells were washed twice with 1× PBS and resuspended in ProLong Gold antifade reagent (Invitrogen).

Protein extraction and purification

Cells were grown in AFM for 16 h and harvested by vacuum filtration. For lysis, 500 mg of cells were resuspended in 1 ml ice-cold lysis buffer (50 mM HEPES-KOH, pH 7.6, 1 M KCl, 1 mM $MgCl_2$, 1 mM ethylene glycol tetraacetic acid (EGTA), 5% glycerol, 0.45% Tween-20, 2× protease inhibitor cocktail). For lysates used to analyze the phosphorylation status of Shs1 by mass spectrometry and Western blot, phosphatase inhibitors (50 mM NaF and 100 mM β-glycerophosphate) were added to the lysis buffer. Cells were lysed by bead-beating with 0.5-mm zirconia/silica beads in a MiniBeadbeater-8 (BioSpec Products, Bartlesville, OK) at top speed for five intervals of 90 s with 30-s rests. Cell lysates were clarified by centrifugation for 10 min at 13,200 rpm. Protein concentrations were determined by Bradford assay.

Number	Name	Sequence
AGO5	Green2.2	TGTAGTTCCCGTCATCTTTG
AGO26	Elm1V1	CCCGTACGCCAACAGAGGAGATG
AGO27	Elm1V2	GTGCAGAACAAAGGGCTCTCGAC
AGO28	Elm1IV1	CAGATCTCGAGTGGCTCTACGTC
AGO37	VG3	ATGTTGGACGAGTCGGAATC
AGO234	V3 NAT1	ACATGAGCATGCCCTGCCCC
AGO235	V2 NAT1	GTGGTGAAGGACCCATCCAG
AGO365	5′ Shs1 tag	CTCCATCTGCCGACTCTAGTC
AGO427	Shs1V2	GCGCCCACAGTAGTGGTTTCAGA
AGO428	Shs1IV1	GCGGCTCTCAGGATAGGACGAA
AGO452	Elm1 Nat F	GACGACAATAGAAAACCAGTTGCATGGTGCTAGGGCATAGGGAGCCGACGGCCAGTGAATTCGAG
AGO453	Elm1 Nat R	CAGACGATTACAAGCGCAGTAGTAACTGCGGTGTGTGTGGGGATGGACCATGATTACGCCAAGCT
AGO520	GFP seqR	CGAGATTCCCGGGTAATAAC
AGO521	Gen seq F	TGGTGTCGCTCCTTCTAGTG
AGO557	Shs1 int seq R	CCCAGTGGAACTGGAAAGAC
AGO593	point mutate PCR V2	GTGTCTCCTCTGCGAGTACC
AGO649	Cdc11-TAP F	GAACGTCTGGAAAAAGAAGCCAAAACCAAGCAGGAAATTGAGGATAAAACGACGGCCAGTGAATTCGAGCTC
AGO650	Cdc11-TAP R	CTAGCGTATGATGCTCACATGTTTCAGCCATTCTTTTCTTGCTTCCAGGCATGCAAGCTTAGATC
AGO651	Cdc11 int F	CACGGGAAGAGCAGATCAGG
AGO652	TAP int R	CATTACGACCGAGATTCCCG
AGO653	TAP ds F	GGACGAGTCGGAATCGCAGAC
AGO654	TAP teft2 R	CAGGCATGCAAGCTTAGATC
AGO684	Shs1 PM seq 1 R	GAGCCATTCCGTTTCTGTTG
AGO775	Shs1-6A-GFP-Gen R	GCAAACCGCCTCTCCCCGCGCGTTGGCCGATTCATTAATGCCGCGTTCTGTTACATACCC
AGO776	Shs1-6D-GFP Gen R	GGCCAGTGAGCGCGCGTAATACGACTCACTATAGGGCGCCGCGTTCTGTTACATACCC
AGO953	Shs1-GFP-Gen 9PM F	CATCTGCCGACTCTAGTCAATTTGCTAGTGATGGATATGCTTCCCGCGCAACAGG
AGO996	Shs1ΔC GFP Gen F	TTCAAAGGGTACTTCAATAGTAAAGACCGAGAAGAATTCCAAAACGACGGCCAGTGAATTCG
AGO997	Shs1ΔC GFP Gen R	GTCTTATTACCATTATGGTGGGATATCTGCGTATAGACCATGATTACGCCAAGCTTGC
AGO1129	Sc Shs1ΔC GFP Gen F	GTTAAGAAATATTTCAGAAACCGTTCCATATGTCTTGAGACATAAAACGACGGCCAGTGAATTCG
AGO1130	Sc Shs1ΔC GFP Gen R	TTATTTATTTGCTCAGCTTTGGATTTTGTACAGATACAACCATGATTACGCCAAGCTTGC
AGO1061	Shs1ΔCC a F	TGCCGGGTAACGGAAATAAC
AGO1062	Shs1ΔCC b R	ATGTCTCAACACATATGGCAGTGTCTCCG
AGO1063	Shs1ΔCC c F	GTTGAGACATACGACGTCAATAGGATCAACTGTGACC

TABLE 6: Oligonucleotides used in this study.

Septin complexes to be analyzed by mass spectrometry were purified from AG124 (Shs1-GFP) lysates using the GFP-Trap-M system (Chromotek, Munich, Germany). Lysates containing 18 mg total protein were incubated with 12 µl GFP-Trap-M beads for 2 h at 4°C. Beads with precipitated proteins were separated from lysates on a magnet and washed seven times with 150 µl IP wash buffer (50 mM HEPES-KOH, pH 7.6, 200 mM KCl, 1 mM $MgCl_2$, 1 mM EGTA, 5% glycerol, 0.1% Tween-20). Precipitated proteins were eluted in 35 µl 5× reducing sample buffer and separated on a 16 × 18 cm 10% acrylamide gel by SDS–PAGE at 25 mA for 7 h. Proteins were stained using the colloidal-blue staining kit (Invitrogen). Bands representing Shs1p were excised and analyzed for phosphorylation, acetylation, and sumoylation by the Taplin Biological Mass Spectrometry facility (Harvard Medical School, Boston, MA).

Septin complexes to be analyzed for Shs1p phosphorylation by phosphatase treatment were purified from AG495.1 (Cdc11-TAP). Lysates containing 10 mg total protein were incubated with 100 µl protein A–Sepharose beads (Sigma-Aldrich) and 50 µl rabbit

immunoglobulin G (IgG; Fisher) at 4°C for 2 h. Immunoprecipitates were washed twice with IP wash buffer, and samples to be treated with phosphatase were washed twice with 1× phosphatase buffer (New England Biolabs). Samples were treated with λ-phosphatase (New England Biolabs), phosphatase buffer only, or phosphatase buffer with phosphatase inhibitors for 1 h at 30°C. Samples were washed twice with IP wash buffer and eluted in 1× reducing sample buffer. Proteins were separated by SDS–PAGE.

For comparison of septin complexes formed in AG539.2 (Shs1ΔC-GFP) with those in AG124 (Shs1-GFP), lysates containing 7.5 mg total protein were incubated with 50 µl Dynabeads (Invitrogen) coupled to anti-GFP (ab290; Abcam, Cambridge, MA) per the manufacturer's instructions for 2 h at 4°C. Beads were washed three times with wash buffer (100 mM HEPES, pH 8.0, 20 mM Mg acetate, 300 mM Na acetate, 10% glycerol, 10 mM EGTA, 0.1 mM EDTA, 0.5% NP-40) on a magnet and eluted in 1× sample buffer at 65°C for 10 min. Samples were reduced by adding 0.35 µl β-mercaptoethanol (Fisher) and boiling for 5 min. Proteins were separated by SDS–PAGE on a 10% acrylamide gel and silver-stained.

Septin complexes purified for electron microscopy were immunoprecipitated from AG495.1 (Cdc11-TAP). Lysates containing 40 mg total protein were precleared with 500 µl protein A–Sepharose beads for 2 h, which was followed by an incubation with 800 µl protein A–Sepharose beads and 100 µl rabbit IgG for 3 h at 4°C. Beads were transferred to a 0.8 × 4 cm poly-prep chromatography column and washed with 30 ml purification wash buffer (100 mM HEPES, pH 8.0, 20 mM Mg acetate, 300 mM Na acetate, 10% glycerol, 10 mM EGTA, 0.1 mM EDTA, 0.5% NP-40); this was followed by 10 ml TEV cleavage buffer (10 mM Tris HCl, pH 8.0, 150 mM NaCl, 0.1% NP-40, 0.5 mM EDTA, 1.0 mM dithiothreitol). Beads were treated overnight with 300 U ProTEV Protease Plus (Promega, Madison,WI) in 1 ml TEV cleavage buffer. Purified proteins were collected by gravity flow-through and ProTEV Protease Plus was removed from the eluate using Magne-His Ni Particles (Promega). The sample was then split in half, and dialyzed into either 1 M KCl or 75 mM KCl buffer (20 mM HEPES, 1M or 75 mM KCl, 0.5 mM EDTA, 0.5 mM EGTA, 8% sucrose).

Western blotting

Whole-cell extracts or immunoprecipitates were loaded onto a 10% polyacrylamide gel and separated by SDS–PAGE for 60 min at a constant voltage of 165 V. Proteins were transferred to polyvinylidene fluoride (PVDF) membrane (Bio-Rad, Hercules, CA). Membranes were probed with rabbit polyclonal anti-GFP antibody (ab290; Abcam) at a 1:1000, rat monoclonal anti–α-tubulin antibody (AbD; Serotec, Raleigh, NC) both at a 1:1000 dilution, and/or an anti-Shs1 antibody (a gift from Doug Kellogg, University of California, Santa Cruz) at a final concentration of 2 µg/ml. All primary antibodies were diluted in PBS-Tween-20 (0.1%) with 3% milk. Alkaline phosphatase–conjugated secondary antibodies (Bio-Rad) were used at a 1:10,000 dilution in PBS–Tween-20 (0.1%). Blots were developed with the enhanced chemifluorescence detection system and visualized using a Storm 860 PhosphorImager (GE Healthcare, Piscataway, NJ).

Electron microscopy

Freshly isolated and dialyzed septin complex was applied to glow-discharged carbon-coated 300-mesh Cu grids (Electron Microscopy Sciences, Hatfield, PA). After 2 min, the grids were rinsed in water and stained with 1% uranyl acetate in 50% methanol for 30 s. The excess uranyl acetate was wicked away with filter paper. All transmission electron microscopy images were taken at 100 kV on a JEOL TEM1010 equipped with a digital camera (XR-41B) and capture engine software (AMTV540; Advanced Microscopy Techniques, Woburn, MA). Micrographs were captured at 25,000× magnification. Septin complex length measurements were taken in ImageJ (National Institutes of Health).

ACKNOWLEDGMENTS

We thank the Gladfelter lab for useful discussions and careful reading of the manuscript; Cori D'Ausilio for statistical consultation; and Doug Kellogg and Kristin Baetz for protocols and reagents. This work is supported by National Science Foundation grant MCB-0719126 (awarded to A.S.G.), National Science Foundation grant MCB-1212400 (A.S.G), and National Institutes of Health training grant T32 AI007519 (awarded to R.A.M.).

REFERENCES

Altmann-Johl R, Philippsen P (1996). AgTHR4, a new selection marker for transformation of the filamentous fungus Ashbya gossypii, maps in a four-gene cluster that is conserved between A. gossypii and Saccharomyces cerevisiae. Mol Gen Genet 250, 69–80.

Alvarez-Tabares I, Perez-Martin J (2010). Septins from the phytopathogenic fungus *Ustilago maydis* are required for proper morphogenesis but dispensable for virulence. PLoS One 5, e12933.

Amin ND, Zheng YL, Kesavapany S, Kanungo J, Guszczynski T, Sihag RK, Rudrabhatla P, Albers W, Grant P, Pant HC (2008). Cyclin-dependent kinase 5 phosphorylation of human septin SEPT5 (hCDCrel-1) modulates exocytosis. J Neurosci 28, 3631–3643.

Anker JF, Gladfelter AS (2011). Axl2 integrates polarity establishment, maintenance, and environmental stress response in the filamentous fungus Ashbya gossypii. Eukaryot Cell 10, 1679–1693.

Ayad-Durieux Y, Knechtle P, Goff S, Dietrich F, Philippsen P (2000). A PAK-like protein kinase is required for maturation of young hyphae and septation in the filamentous ascomycete *Ashbya gossypii*. J Cell Sci 113, 4563–4575.

Barral Y, Mermall V, Mooseker MS, Snyder M (2000). Compartmentalization of the cell cortex by septins is required for maintenance of cell polarity in yeast. Mol Cell 5, 841–851.

Beise N, Trimble W (2011). Septins at a glance. J Cell Sci 124, 4141–4146.

Bertin A, McMurray MA, Grob P, Park SS, Garcia G, III, Patanwala I, Ng HL, Alber T, Thorner J, Nogales E (2008). *Saccharomyces cerevisiae* septins: supramolecular organization of heterooligomers and the mechanism of filament assembly. Proc Natl Acad Sci USA 105, 8274–8279.

Bertin A, McMurray MA, Thai L, Garcia G, III, Votin V, Grob P, Allyn T, Thorner J, Nogales E (2010). Phosphatidylinositol-4,5-bisphosphate promotes budding yeast septin filament assembly and organization. J Mol Biol 404, 711–731.

Casamayor A, Snyder M (2003). Molecular dissection of a yeast septin: distinct domains are required for septin interaction, localization, and function. Mol Cell Biol 23, 2762–2777.

de Almeida Marques I, Valadares NF, Garcia W, Damalio JC, Macedo JN, de Araujo AP, Botello CA, Andreu JM, Garratt RC (2012). Septin C-terminal domain interactions: implications for filament stability and assembly. Cell Biochem Biophys 62, 317–328.

DeMay BS, Bai X, Howard L, Occhipinti P, Meseroll RA, Spiliotis ET, Oldenbourg R, Gladfelter AS (2011). Septin filaments exhibit a dynamic, paired organization that is conserved from yeast to mammals. J Cell Biol 193, 1065–1081.

DeMay BS, Meseroll RA, Occhipinti P, Gladfelter AS (2009). Regulation of distinct septin rings in a single cell by Elm1p and Gin4p kinases. Mol Biol Cell 20, 2311–2326.

DeMay BS, Meseroll RA, Occhipinti P, Gladfelter AS (2010). Cellular requirements for the small molecule forchlorfenuron to stabilize the septin cytoskeleton. Cytoskeleton (Hoboken) 67, 383–399.

Dietrich FS *et al*. (2004). The *Ashbya gossypii* genome as a tool for mapping the ancient *Saccharomyces cerevisiae* genome. Science 304, 304–307.

Egelhofer TA, Villen J, McCusker D, Gygi SP, Kellogg DR (2008). The septins function in G1 pathways that influence the pattern of cell growth in budding yeast. PLoS One 3, e2022.

Field CM, al-Awar O, Rosenblatt J, Wong ML, Alberts B, Mitchison TJ (1996). A purified *Drosophila* septin complex forms filaments and exhibits GTPase activity. J Cell Biol 133, 605–616.

Frazier JA, Wong ML, Longtine MS, Pringle JR, Mann M, Mitchison TJ, Field C (1998). Polymerization of purified yeast septins: evidence that

organized filament arrays may not be required for septin function. J Cell Biol 143, 737–749.
Garcia G, III, Bertin A, Li Z, Song Y, McMurray MA, Thorner J, Nogales E (2011). Subunit-dependent modulation of septin assembly: budding yeast septin Shs1 promotes ring and gauze formation. J Cell Biol 195, 993–1004.
Gladfelter AS, Hungerbuehler AK, Philippsen P (2006). Asynchronous nuclear division cycles in multinucleated cells. J Cell Biol 172, 347–362.
Gladfelter AS, Pringle JR, Lew DJ (2001). The septin cortex at the yeast mother-bud neck. Curr Opin Microbiol 4, 681–689.
Gonzalez-Novo A, Correa-Bordes J, Labrador L, Sanchez M, Vazquez de Aldana CR, Jimenez J (2008). Sep7 is essential to modify septin ring dynamics and inhibit cell separation during *Candida albicans* hyphal growth. Mol Biol Cell 19, 1509–1518.
Hagiwara A, Tanaka Y, Hikawa R, Morone N, Kusumi A, Kimura H, Kinoshita M (2011). Submembranous septins as relatively stable components of actin-based membrane skeleton. Cytoskeleton (Hoboken) 68, 512–525.
Hartwell LH (1971). Genetic control of the cell division cycle in yeast. IV. Genes controlling bud emergence and cytokinesis. Exp Cell Res 69, 265–276.
Helfer H, Gladfelter AS (2006). AgSwe1p regulates mitosis in response to morphogenesis and nutrients in multinucleated *Ashbya gossypii* cells. Mol Biol Cell 17, 4494–4512.
Hernandez-Rodriguez Y, Hastings S, Momany M (2012). The septin AspB in Aspergillus nidulans forms bars and filaments and plays roles in growth emergence and conidiation. Eukaryot Cell 11, 311–323.
Ihara M *et al.* (2007). Sept4, a component of presynaptic scaffold and Lewy bodies, is required for the suppression of α-synuclein neurotoxicity. Neuron 53, 519–533.
Iwase M, Luo J, Bi E, Toh-e A (2007). Shs1 plays separable roles in septin organization and cytokinesis in *Saccharomyces cerevisiae*. Genetics 177, 215–229.
Johnson ES, Blobel G (1999). Cell cycle-regulated attachment of the ubiquitin-related protein SUMO to the yeast septins. J Cell Biol 147, 981–994.
Kaufmann A (2009). A plasmid collection for PCR-based gene targeting in the filamentous ascomycete *Ashbya gossypii*. Fungal Genet Biol 46, 595–603.
Kinoshita A, Kinoshita M, Akiyama H, Tomimoto H, Akiguchi I, Kumar S, Noda M, Kimura J (1998). Identification of septins in neurofibrillary tangles in Alzheimer's disease. Am J Pathol 153, 1551–1560.
Kinoshita M, Field CM, Coughlin ML, Straight AF, Mitchison TJ (2002). Self- and actin-templated assembly of mammalian septins. Dev Cell 3, 791–802.
Li CR, Yong JY, Wang YM, Wang Y (2012). CDK regulates septin organization through cell-cycle-dependent phosphorylation of the Nim1-related kinase Gin4. J Cell Sci 125, 2533–2543.
Lindsey R, Ha Y, Momany M (2010). A septin from the filamentous fungus *A. nidulans* induces atypical pseudohyphae in the budding yeast *S. cerevisiae*. PLoS One 5, e9858.
Longtine MS, Fares H, Pringle JR (1998). Role of the yeast Gin4p protein kinase in septin assembly and the relationship between septin assembly and septin function. J Cell Biol 143, 719–736.
Luedeke C, Frei SB, Sbalzarini I, Schwarz H, Spang A, Barral Y (2005). Septin-dependent compartmentalization of the endoplasmic reticulum during yeast polarized growth. J Cell Biol 169, 897–908.
McMurray MA, Bertin A, Garcia G, III, Lam L, Nogales E, Thorner J (2011a). Septin filament formation is essential in budding yeast. Dev Cell 20, 540–549.
McMurray MA, Stefan CJ, Wemmer M, Odorizzi G, Emr SD, Thorner J (2011b). Genetic interactions with mutations affecting septin assembly reveal ESCRT functions in budding yeast cytokinesis. Biol Chem 392, 699–712.
Mitchell L, Lau A, Lambert JP, Zhou H, Fong Y, Couture JF, Figeys D, Baetz K (2011). Regulation of septin dynamics by the *Saccharomyces cerevisiae* lysine acetyltransferase NuA4. PLoS One 6, e25336.
Mortensen EM, McDonald H, Yates J, III, Kellogg DR (2002). Cell cycle-dependent assembly of a Gin4-septin complex. Mol Biol Cell 13, 2091–2105.
Mostowy S, Cossart P (2012). Septins: the fourth component of the cytoskeleton. Nat Rev Mol Cell Biol 13, 183–194.
Nagaraj S, Rajendran A, Jackson CE, Longtine MS (2008). Role of nucleotide binding in septin-septin interactions and septin localization in *Saccharomyces cerevisiae*. Mol Cell Biol 28, 5120–5137.
Oh Y, Bi E (2011). Septin structure and function in yeast and beyond. Trends Cell Biol 21, 141–148.
Peterson EA, Petty EM (2010). Conquering the complex world of human septins: implications for health and disease. Clin Genet 77, 511–524.
Rodal AA, Kozubowski L, Goode BL, Drubin DG, Hartwig JH (2005). Actin and septin ultrastructures at the budding yeast cell cortex. Mol Biol Cell 16, 372–384.
Schmitz HP, Kaufmann A, Kohli M, Laissue PP, Philippsen P (2006). From function to shape: a novel role of a formin in morphogenesis of the fungus *Ashbya gossypii*. Mol Biol Cell 17, 130–145.
Sikorski RS, Hieter P (1989). A system of shuttle vectors and yeast host strains designed for efficient manipulation of DNA in *Saccharomyces cerevisiae*. Genetics 122, 19–27.
Sinha I, Wang YM, Philp R, Li CR, Yap WH, Wang Y (2007). Cyclin-dependent kinases control septin phosphorylation in *Candida albicans* hyphal development. Dev Cell 13, 421–432.
Sirajuddin M, Farkasovsky M, Hauer F, Kuhlmann D, Macara IG, Weyand M, Stark H, Wittinghofer A (2007). Structural insight into filament formation by mammalian septins. Nature 449, 311–315.
Takizawa PA, DeRisi JL, Wilhelm JE, Vale RD (2000). Plasma membrane compartmentalization in yeast by messenger RNA transport and a septin diffusion barrier. Science 290, 341–344.
Tang CS, Reed SI (2002). Phosphorylation of the septin cdc3 in g1 by the cdc28 kinase is essential for efficient septin ring disassembly. Cell Cycle 1, 42–49.
Wendland J, Ayad-Durieux Y, Knechtle P, Rebischung C, Philippsen P (2000). PCR-based gene targeting in the filamentous fungus *Ashbya gossypii*. Gene 242, 381–391.
Wightman R, Bates S, Amornrrattanapan P, Sudbery P (2004). In *Candida albicans*, the Nim1 kinases Gin4 and Hsl1 negatively regulate pseudohypha formation and Gin4 also controls septin organization. J Cell Biol 164, 581–591.